Working Report 2012-28

REDUPP
First Annual Report

Editors:

Lena Zetterström Evins

Marjut Vähänen

June 2012

POSIVA OY
FI-27160 OLKILUOTO, FINLAND
Tel +358-2-8372 31
Fax +358-2-8372 3709

Working Report 2012-28

REDUPP
First Annual Report

Editors:

Lena Zetterström Evins

Svensk Kärnbränslehantering AB (SKB)

Marjut Vähänen

Posiva Oy

June 2012

ABSTRACT

The REDUPP project aims to investigate how surfaces of solids with a fluorite structure change with time during dissolution. Laboratory experiments are performed to monitor dissolution of CaF_2, CeO_2, ThO_2 and UO_2, in connection with ab initio calculations. Another aspect of the project involves investigating if using natural groundwater in the leaching tests has an effect on the measured dissolution rate of UO_2. The preliminary results after one project year are documented here. Samples have been prepared as sintered pellets with similar microstructures as UO_2. For the UO_2 study, pellets doped with ^{233}U are used. Preliminary dissolution data show the expected trends for pH and temperature dissolution kinetics dependence. Studies on CeO_2 monolith samples indicate that there is a crystallographic control on leaching, and that the grain boundaries are preferentially attacked. Measurable Th concentrations are achieved in pre-tests for ThO_2 dissolution where the effect of carbonate complexation is also observed. The preliminary results of the studies performed on ^{233}U-doped UO_2 samples in natural groundwater are in agreement with previous results, and show no observable effect of trace elements or level of alpha radiolysis. In the modelling work, the stabilities of surfaces corresponding to different crystal planes have been computed, and work is in progress to develop a model involving stepped surfaces. Preliminary results show that only a few energies of reference planes need to be computed, and all other surface energies can be accurately estimated from a linear relation. The goal is to develop a model of how the surfaces of fluorite-structures evolve during dissolution.

Keywords: Fluorite, CeO_2, ThO_2, UO_2, Dissolution, Surfaces, Crystal Planes, Modelling.

REDUPP -projektin vuosiraportti 2011-2012

TIIVISTELMÄ

EU-projektissa REDUPP tutkitaan, miten fluoriittirakenteen omaavien kiinteiden aineiden pinta muuttuu liukenemisen aikana. Laboratoriokokeiden ja ab initio - laskelmien avulla tutkitaan CaF_2, CeO_2, ThO_2 ja UO_2 –yhdisteiden liukenemista. Projektissa tutkitaan myös luonnon pohjavesikoostumuksen vaikutusta mitattuun UO_2:n liukenemisnopeuteen alfa-radiolyysiolosuhteissa. Tässä raportissa esitellään REDUPP-projektin alustavat tulokset ensimmäisen vuoden ajalta. Tutkittaviksi faaseiksi valmistettiin sintrattuja CaF_2, CeO_2, ThO_2-pellettejä, joilla on samanlainen mikrorakenne kuin UO_2:lla. UO_2 tutkimuksessa tehdään liukenemiskokeita ^{233}U- doupatuilla uraanidioksidi faaseilla.

Alustavat tulokset osoittavat liukenemiskinetiikan olevan riippuvainen pH:sta ja lämpötilasta, mikä oli odotettavissa. CeO_2 jauheen liukenemiskokeissa saadut alustavat tulokset ovat yhtäpitäviä aikaisempien Ce:ia sisältävien oksidien kokeiden tulosten kanssa. CeO_2 monoliittinäytteiden tutkimukset osoittavat, että kristallografia kontrolloi liukenemista (eluutiota) ja että raerajat reagoivat ensisijaisesti. ThO_2 –liukoisuuskokeissa Th –pitoisuudet olivat mitattavissa. Lisäksi havaittiin, että karbonaatti-kompleksaatio vaikutti liuokoisuuteen. Luonnon pohjavedessä käynnistettyjen ^{233}U-doupattujen UO_2 faasien liukenemiskokeiden alustavat tulokset ovat samansuuntaisia kuin aikaisemmin simuloidussa pohjavedessä saadut tulokset. Alfa-radiolyysin tai hivenaineiden vaikutusta ei havaittu lyhyillä koeajoilla.

Mallinnuksen avulla laskettiin eri kidetasoja vastaavien pintojen stabiilisuutta. Työ on käynnissä askelmia sisältävävien pintojen mallin kehittämiseksi. Alustavien tulosten mukaan vain muutamia pinta-energioita pitää laskea eri referenssitasoille ja kaikki muut pinta-energiat voidaan arvioida tarkasti lineaaristen riippuvuuksien avulla. Tavoitteena on kehittää malli sille, kuinka fluoriitti-pinnat kehittyvät liukenemisen aikana.

Avainsanat: Fluoriitti, CeO_2, ThO_2, UO_2, liukeneminen, pinnat, kidetasot, mallintaminen.

TABLE OF CONTENT

FOREWORD/PREFACE

The project Reducing Uncertainty in Performance Prediction (REDUPP) is a 36 months (April 2011 – April 2014) Collaborative Project under the Seventh Framework Programme of the European Atomic Energy Community (EURATOM). The activity area is "Management of radioactive waste".

The participant organisations are:
Svensk Kärnbränslehantering AB (SKB), University of Sheffield (USFD), Uppsala University (UU), VTT Technical Research Centre of Finland (VTT) and Posiva.

This report summarizes the results of the first project year.

The contributors to this report are the following:

Martin Stennett (USFD)
Claire Corkhill (USFD)
Daniel Bailey (USFD)
Neil Hyatt (USFD)
Pablo Maldonado (UU)
Peter Oppeneer (UU)
Emmi Myllykylä (VTT)
Kaija Ollila (VTT)
Marjut Vähänen, Posiva Oy (Editor)
Lena Zetterström Evins, SKB (Editor)

We are grateful for the reviews and helpful discussions with the REDUPP Scientific Advisory Board: Virginia Oversby (VMO Konsult), Chris Hall (University of Edinburgh) and Javier Giménez (UPC).

1 INTRODUCTION

1.1 Overall aim

The project aims to investigate how surfaces of solids with a fluorite structure – UO_2, ThO_2, CeO_2 and CaF_2 – change with time during dissolution, and how those changes affect the dissolution rate. Laboratory experiments monitoring dissolution of crushed synthetic material will be performed, in connection with first principles (ab initio) calculations. The experimental data will guide the calculations, and vice versa, to develop a computational model of how the surfaces of fluorite-structures evolve during dissolution.

The final aim of the REDUPP project is to reduce the uncertainties in the spent nuclear fuel dissolution rates used when assessing the long-term safety of geological disposal concepts of nuclear waste.

1.2 Scientific background

There is a need to improve our understanding of interactions between solid surface and fluid during the dissolution process; it is the goal of this project to improve this situation, and to reduce the uncertainties involved. The combination of dissolution testing, surface characterisation, and theoretical modelling of the dissolution process will bring us one step closer to understanding the long-term changes in dissolution rate of spent nuclear fuel.

Through controlled laboratory experiments, the fractional dissolution rate of spent nuclear fuel has been estimated to be in the range of 10^{-6} to 10^{-8} per year, meaning complete dissolution of all spent fuel would take about 10 million years (SKB, 2010). Even though this may seem like a slow rate it is clear that it is faster than rates deduced from observations of uranium ores. There are plenty of examples of uranium oxide ores that have persisted for many hundreds of millions of years, and even over a billion years (e.g. Smellie & Karlsson 1996; Gauthier-Lafaye et al. 1996), thus implying that the dissolution rates in those ores have been much slower than 10^{-7} per year. Ollila and Oversby (2005) performed dissolution experiments to determine an upper limit to the dissolution rate of UO_2 under reducing conditions appropriate to those in a geologic repository for spent fuel disposal in Finland and Sweden. Test duration ranged from 52 to 140 days; from these results, fractional dissolution rates (not related to surface area) were obtained. The findings indicated a trend towards slower dissolution rates as the samples were exposed to sequential testing periods, indicating a surface maturation analogous to that of weathered minerals in a natural setting as described by White and Brantley (2003). The rates measured in the laboratory may well be influenced by transient effects such as high-energy surface sites, which implies that the dissolution rates measured are upper limits. Ollila and Oversby (2005) observed also that the radiolysis effect of varying amount of ^{233}U in the studied samples was negligible compared to the differences between duplicate samples; this indicates that defects in the samples such as high energy surface sites are much more important than any effects due to alpha radiolysis.

The observation that laboratory dissolution rates are, in general, faster than what is estimated from analyses of materials in nature in not a new one; White and Brantley (2003) provide an overview of this, and discuss some reasons why 'time-dependent weathering rates' occur. They remark that the effects of time can be seen not only in the discrepancy between experimental and natural weathering rates, but also in systematic decreases in natural rates in progressively older weathering environments. Thus, in both nature and in the laboratory, the surface of a reacting mineral appears to adjust so that dissolution rates slow down with reaction time. The reasons for this may be manifold. There are both intrinsic and extrinsic factors; intrinsic factors are physical and chemical properties of the mineral that may change with time during weathering, while extrinsic features are environmental conditions that may also change with time and impact the chemical weathering rate (White and Brantley 2003).

The REDUPP project addresses these issues by carefully documenting the solid-state characteristics of the samples before dissolution, and monitoring the rate and surface changes during dissolution. The effect of external factors is addressed by using natural groundwater, adding chemical complexity of the solution.

1.3 Summary of the project activities

The project activities are divided into different Work Packages (WPs), most of which are concerned with dissolution experiments and surface characterisation of a suite of materials with the same crystal structure: CaF_2, CeO_2, ThO_2 and UO_2. One Work package (WP 4) addresses the effect of the complexity of natural groundwater on UO_2 dissolution rates. A central part of the project is the first-principles modelling, which is performed in WP 6. WP 7 and WP 8 are concerned with coordination and management.

One of the project goals is to determine how the "ageing" of the sample surface affects the measured dissolution rate. We can approach the long-term dissolution rate in the laboratory, but we cannot at this time estimate how far away we are from it. By using first-principles calculations and computational modelling, a model of how the surface evolves during dissolution can be produced. Within the project, young scientists will be trained and receive mentoring. The project will interact with PhD-students in associated networks, and provide a lecture series, and thus introduce students to the needs of the nuclear community in Europe. New knowledge which arises from the project will be communicated to a wider audience through a web page, newsletters and a final open meeting.

The apparent discrepancy between rates in laboratory and in nature is addressed in this project by investigating processes at the solid-liquid interface. One expected result is a reduced uncertainty regarding the dissolution process, through a deeper understanding of surface changes during dissolution. The studied materials have very low solubility and analysed solutions will therefore contain very low amounts of the elements of interest. Analytical data of high quality is attained through analyses by High Resolution ICP-MS; thereby this project will also contribute to method development, personnel training and improvement of data bases. The results are communicated to a wide audience through a series of reports and in several scientific journal articles; the project

web page and the newsletters will inform the public and interested organisations of the progress of the project. The aim is to present a general model that would then be available for application in further research concerning nuclear fuel dissolution.

2 SYNTHESIS AND CHARACTERISATION OF CeO_2 (WP 1)

By Martin C. Stennett, Claire L. Corkhill, and Neil C. Hyatt
University of Sheffield.

2.1 Introduction

The use of spent nuclear fuel or its main component, UO_2, in laboratory dissolution experiments is problematic due to issues surrounding radioactivity and redox sensitivity. Uranium is stable in its U(IV) oxidation state as UO_2 under reducing conditions, such as those likely to prevail in deep geological repositories. However, in the presence of oxygen, uranium oxidises to the readily soluble uranyl (UO_2^{2+}) U(VI) form. In dissolution experiments with UO_2, anoxic, reducing conditions are maintained through exclusion of oxygen from the air and extensive pre-treatment with leaching solutions is conducted to remove any oxidised material from the sample surfaces (Ollila and Oversby, 2005). This may also include the addition of a corroding Fe-strip to prevent any oxygen in solution reaching the UO_2 surface (Ollila 2008a). The redox sensitivity of UO_2 prevents the use of normal surface characterisation methods because the exposure of the sample to even trace amounts of oxygen would alter the sample surface. It is, therefore, necessary to produce suitable non-radioactive, non-redox sensitive analogues that closely resemble nuclear fuel in terms of crystallography and microstructure so that we can gain a better understanding of how changes in the surface sample surface affect dissolution rates measured in the laboratory.

Such an analogue should have the same fluorite crystal structure as UO_2 (face centred cubic, space group Fm3m). This is common in other f-block oxides, notably the rare-earth element cerium, CeO_2 (Atlas and Tel 2001) and also the actinide thorium, ThO_2. The archetypal fluorite structure occurs in CaF_2. The analogue must also have a microstructure similar to that of a typical UO_2 nuclear fuel; the grains should be randomly orientated (Godhino et al. 2011) and have a specific size and porosity. This is determined by the burn-up conditions of the fuel, for example, porosity increases with increasing burn-up (Romano et al. 2007). The ideal composition and resulting microstructures of an analogue material can be achieved through varying the calcination and sintering temperatures of the starting material.

In this study, we detail the methodology used to prepare CeO_2 analogue ceramics for UO_2 and provide a detailed characterisation of the morphology, crystallography and chemistry of the surfaces of the samples. Calcination and sintering temperatures were optimised to yield particle size distributions and surface areas close to those used in UO_2 manufacture. Information regarding ThO_2 and CaF_2 pellet synthesis and characterisation is found in REDUPP Deliverable 1.1, which is available on the REDUPP web site (www.skb.se/REDUPP).

2.2 Methodology

CeO_2 powders were prepared via thermal decomposition of cerium (IV) oxalate, $Ce(C_2O_4)_2.xH_2O$. Thermal decomposition of the oxalate was conducted for one hour at 400 °C, 550 °C and 800 °C (5 °C min^{-1} ramp rate) to derive three CeO_2 powders with different powder properties. The composition of the powders were confirmed using X-Ray Diffraction (XRD). The powder densities were measured using a pycnometer, surface area analysis was conducting using the BET method, and the powder particle size was measured with a laser particle sizer.

CeO_2 powders were uniaxially pressed in a 10 mm diameter hardened stainless steel die and the densities of the green compacts were calculated from the pellet mass and geometry. Green CeO_2 pellets were then sintered in triplicate, for 4 hours, at temperatures between 1300 °C and 1750 °C in a standard air atmosphere muffle furnace. Sintered densities were measured by both geometric and water immersion (Archimedes) methods. The microstructure of these pellets were analysed using Scanning Electron Microscopy (SEM).

Once the optimised temperatures for decomposition (calcination) and sintering were determined, the optimised sintered pellets were subject to Electron Backscatter Diffraction analysis to determine the crystallographic orientation of the grains.

2.3 Results

In order to confirm the full decomposition of the cerium oxalate at each calcination X-ray diffraction was performed. Analysis of the diffraction confirmed full decomposition had occurred at each temperature forming fluorite structured CeO_2 (Figure 2-1).

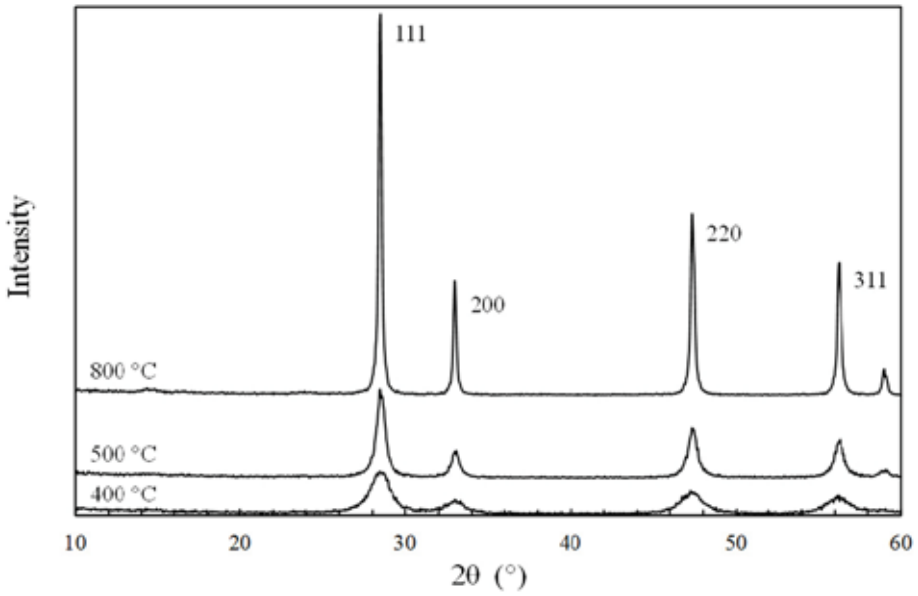

Figure 2-1*. XRD patterns for cerium dioxide powders formed from decomposition of cerium oxalate at 400 °C, 550 °C and 800 °C. All reflections observed were indexed based on cubic CeO_2 with space group Fm-3m.*

The powder properties are shown in Table 2-1. The reactivity of a powder is influenced by its surface area and it was expected that the cerium oxalate calcined at lower temperature would yield more reactive CeO_2 powders which would sinter to higher density at lower temperatures. The powder density of the CeO_2 powders was shown to increase with increasing calcination temperature (Table 2-1) reaching almost theoretical at 800 °C. This is consistent with the observed decrease in surface area. As it gave the largest particle size and the density closest to the theoretical value, the powder calcined at 800 °C was selected for the preparation of sintered CeO_2 pellets.

Table 2-1. *Summary of powder data for cerium oxalate and CeO_2 powders (ρ_{theo} = 7.215 g cm^{-3}). $d_{90\%}$ value represents the particle size that 90% of the particles are less than. Values in parantheses are the estimated standard deviation in the last decimal place.*

Powder	Calcination temperature (°C)	Powder density (g cm^{-3})	Particle size $d_{90\%}$ (μm)	Specific surface area (m^2 g^{-1})
$Ce_2(C_2O_4)_3.xH_2O$	n/a	1.992(1)	25.4(1)	0.4(1)
CeO_2	400	6.320(1)	14.0(1)	90.9(1)
CeO_2	550	6.514(2)	13.9(1)	29.7(1)
CeO_2	800	7.121(5)	23.5(1)	6.93(1)

Pellets derived from the 800 °C calcine and sintered at 1700 °C gave the highest density, > 96 % of theoretical. This combination of calcination and sintering temperatures also gave rise to the greatest grain size (between 5 μm and 20 μm in diameter) and the lowest porosity, as shown in Figure 2-2.

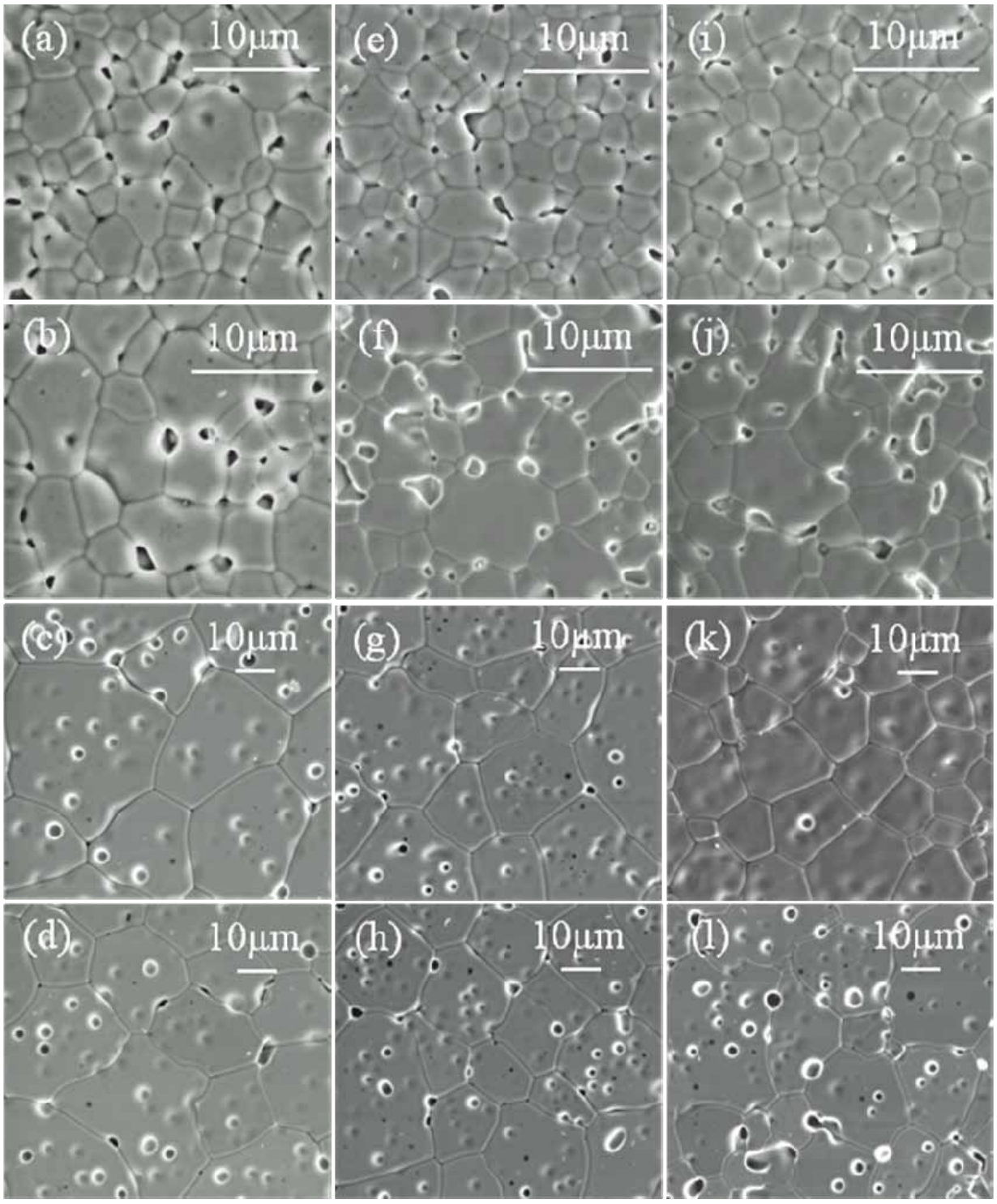

***Figure 2-2**. SEM images of sintered pellets: (a – d) 400 °C oxalate calcination (e – h) 550 °C oxalate calcination and (I - l) 800 °C oxalate calcination. Increasing sintering temperature from top to bottom (1500 °C, 1600 °C, 1700 °C, 1750 °C).*

EBSD confirmed that the CeO_2 synthesis process using powder calcined at 800 °C and sintered at 1700 °C, imaged in Figure 2-2 (k), produced grains had a random crystallographic orientation. The grains are randomly orientated in the major (111), (100) and (110) crystal planes. The average grain diameter, as measured by EBSD, was 8.2 μm.

2.4 Summary

The aim of this work was to fabricate pellets of CeO2 with similar microstructures as UO_2 to act as analogues for dissolution studies. It was possible to produce ceramic bodies with densities in excess of 96 % theoretical by using CeO2 calcined from cerium oxalate at 800 °C and sintering pressed pellets at 1700 °C. The microstructure consisted of equiaxed, randomly orientated grains in the size range between 5 μm and 20 μm. These microstructures are in good agreement with those published on UO_2 fuel (Forsyth 1987 and Forsyth 1995).

3 DISSOLUTION OF CeO_2 POWDERS (WP2)

By Claire L. Corkhill and Neil C. Hyatt
University of Sheffield.

3.1 Introduction

In the safety case for the geological disposal of nuclear waste, the release of radioactivity from the repository is controlled by the dissolution of the spent fuel in groundwater (Shoesmith 2000). Therefore, to assess the performance of the repository after infiltration of groundwater and contact with spent fuel, the dissolution characteristics must be determined. In this preliminary investigation, CeO_2 analogues, prepared as described in Chapter 2, were powdered and were subjected to a range of aggressive and environmentally relevant alteration media with different solubility controls. Dissolution was monitored through analysis of the aqueous solution.

3.2 Experimental methods

CeO_2 was ground to a powder (75 – 150 μm) according to the product consistency test ASTM standard (ASTM C 1285-02). Prior to use, the powder was inspected by SEM to ensure no fine particles >1 μm in size remained. 0.1 g of powder was placed in 50 ml PTFE vessels and filled with 40 ml of alteration solution, either: 0.01 M HNO_3 (pH 2); a simplified groundwater of dilute NaCl (10mM) buffered to pH 8.5 by $NaHCO_3$ (2mM); or 0.005M NaOH (pH 11.7), giving a surface area to volume ratio of 200 m^{-1}. Experiments were performed in triplicate at 70 °C and 90 °C. Sampling was conducted at 0, 1, 3, 7, 14, 21, 28, 35, 42, 56 and 70 days. An aliquot (1.2 ml) of each sample was removed prior to analysis by ICP-MS. Leaching is expressed as the normalised elemental leaching $N_L(Ce)$ (g m^{-2}) according to:

$$N_L(Ce) = \frac{m_{Ce}}{S/V} \tag{3-1}$$

where m_{Ce} is the total amount of Ce released in the solution and S/V is the mineral surface area to solution volume ratio. The normalised element leaching rate $R_L(Ce)$ (g m^{-2} d^{-1}) is determined by:

$$R_L(Ce) = \frac{m_{Ce}}{\frac{S}{V} \times \Delta t} \tag{3-2}$$

where Δt is the leaching time in days.

3.3 Preliminary Results

The normalised leaching of CeO_2 at 90 °C as function of pH is shown in Figure 3-1. Fast initial kinetic leaching (R_L0) is observed for pH 2, pH 8.5 and pH 11.7 batch experiments, with rates of (1.98 ± 0.5) x 10^{-4} g m^{-2} d^{-1}, (0.6 ± 0.1) x 10^{-4} g m^{-2} d^{-1} and (0.50 ± 0.09) x 10^{-4}, respectively (Table 3-1). Under the redox and pH conditions of these experiments, Ce(IV) is the dominant Ce species.

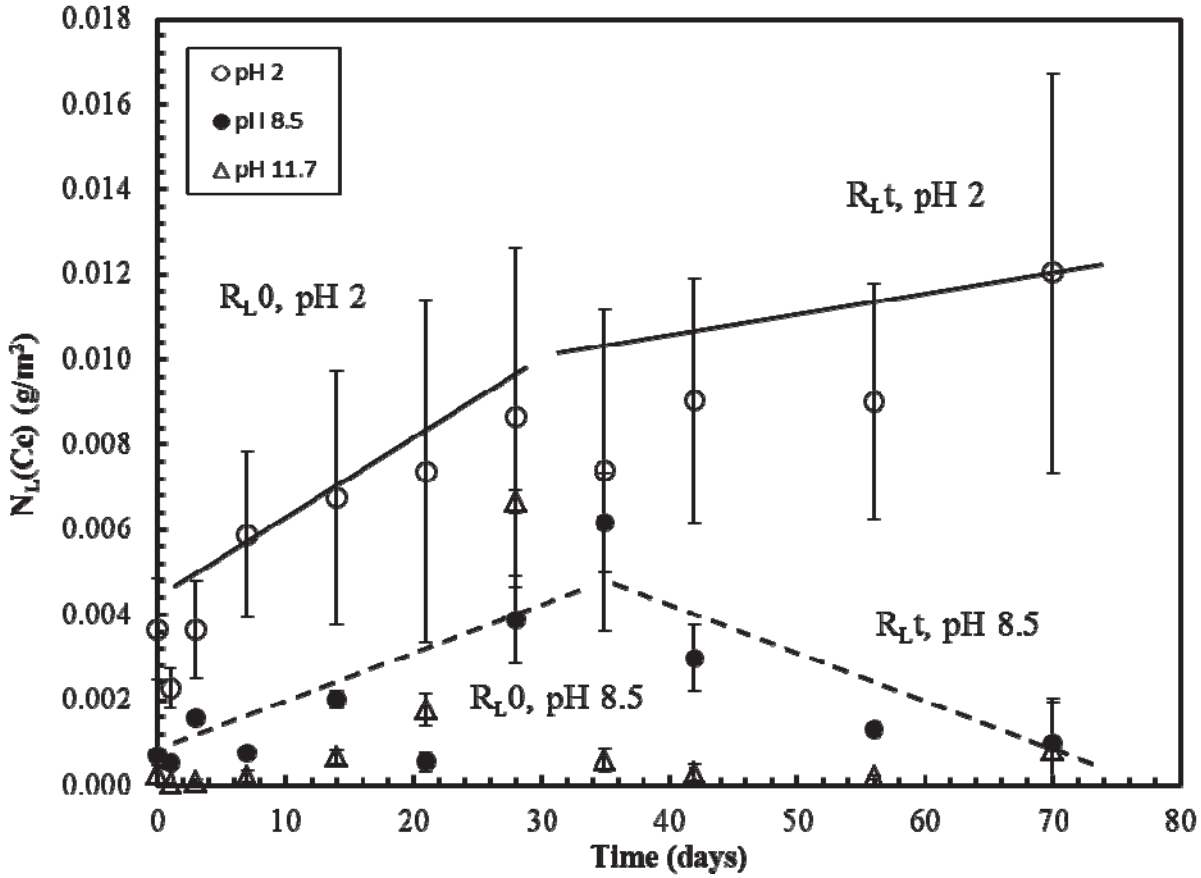

***Figure 3-1**. Normalised leaching $N_L(Ce)$ obtained during leaching tests (T = 90 °C, pH 2 = 0.01M HNO_3, pH 8.5 = NaCl (10mM) / $NaHCO_3$ (2mM) and pH 11.7 = 0.005M NaOH) of crushed CeO_2 (75-150 μm). R_L0 indicates the fast initial kinetic dissolution, and R_Lt indicates the slower solution saturation limited dissolution rate. Rate data are given in Table 3-1.*

At pH 2, as the solution becomes saturated, the concentration of Ce in solution continues to increase, but the leaching rate (R_Lt) decreases (Table 3-1). However, for powders reacted at pH 8.5 and pH 11.7, the leach rate due to saturation (RLt) is also influenced by removal of Ce from solution, most likely through precipitation of $Ce(OH)_4$. Figure 3-2 shows the evolution of normalised leaching of CeO_2 at 70 °C and 90 °C. As expected, for powders reacted at pH 2, the initial kinetic normalised leaching rates (R_L0) are greater than those for 70 °C (Table 3-1). The same trend is observed for powders leached at pH 8.5 and pH 11.7, although the normalised leaching rates are considerably lower (Table 3-1).

***Table 3-1**. Normalised leaching rates for CeO_2 dissolution. R_L0 indicates the fast initial kinetic dissolution and R_Lt indicates the slower solution saturation limited dissolution rate. The latter rate is not given for 70 °C, as these experiments are underway.*

Solution	pH	Alteration temperature (°C)	R_L0 (g m^{-2} d^{-1})	R_Lt (g m^{-2} d^{-1})
HNO_3	2	90	$(1.98 \pm 0.5) \times 10^{-4}$	$(0.10 \pm 0.02) \times 10^{-4}$
HNO_3	2	70	$(0.90 \pm 0.4) \times 10^{-4}$	-
NaCl/$NaHCO_3$	8.5	90	$(0.60 \pm 0.1) \times 10^{-4}$	$(0.02 \pm 0.003) \times 10^{-4}$
NaCl/$NaHCO_3$	8.5	70	$(0.26 \pm 0.06) \times 10^{-4}$	-
NaOH	11.7	90	$(0.50 \pm 0.09) \times 10^{-4}$	$(0.01 \pm 0.001) \times 10^{-4}$
NaOH	11.7	70	$(0.07 \pm 0.005) \times 10^{-4}$	-

These results are significantly lower than those of other leaching tests of multi-component Ce-containing ceramic oxides (e.g. Claparede et al., 2011), which give rates of approximately 3×10^{-3} g m^{-2} d^{-1}. This is most likely due to the low solubility and highly refractory nature of pure CeO_2.

3.4 Summary and future work

These preliminary dissolution data show the expected trends for pH and temperature dissolution kinetics dependence.

Further work will focus on the effect of high energy sites within the material structure, using different sized crushed powders, giving different densities of high energy sites. In conjunction with surface analytical techniques, this work will provide a detailed description of the evolution of surface morphology and the aqueous solution chemistry as dissolution occurs.

4 DISSOLUTION OF ThO_2 (WP3)

By Emmi Myllykylä, VTT

4.1 Introduction

Thoria (ThO_2 (s)), also called thorianate, is a white solid with fluorite structure (space group: Fm3m). Unlike UO_2, thorium dioxide is not redox sensitive. However, ThO_2 is somewhat hygroscopic and has the highest melting point (3300 °C) of all oxides. The sintered thorium oxide is also one of the most refractory substances known (Morss et al. 2010).

Compared to the solubility of UO_2 (cr) in anaerobic conditions (10^{-8} to 10^{-10} mol/L, (Ollila 2008a)), the solubility of ThO_2 is at the same level or even lower. According to the literature, aqueous nitric acid with few percentage of HF or sodium fluorosilicate can provide reasonable amount of Th in solution (Morss et al. 2010).

In contrast to redox active uranium, thorium has only one prevailing oxidation state Th(IV) in natural conditions. As a largest tetravalent actinide ion, Th^{4+} is also the least hydrolysable actinide ion. Th^{4+} is the prevailing form of thorium in water solutions from pH 1 to 4. The Th^{4+} ion has a tendency to undergo polynucleation and colloid formation. From pH 4 Th^{4+} starts to form hydroxides and hydrous oxides, which also have relatively low solubility. As a large tetravalent ion Th^{4+} forms generally weak complexes. However it has moderately strong complexes with fluoride, sulphate, phosphate and carbonate which all may increase the solubility of thorium. In aquatic environments, the carbonate complex formation is especially important and has been shown to affect the thorium solubility (Morss et al. 2010; Lehto and Hou 2011).

The solubility values for ThO_2, as well as hydrolysis constants for thorium show great discrepancies in literature (Vandenborre et al. 2010). The main reasons for variation are the tendency to undergo polynucleation and colloid formation, strong absorption to surfaces, and the low solubility of Th^{4+} hydroxide and hydrous oxide. Figure 4-1 shows the solubility curves for crystalline thorium dioxide and amorphous $Th(OH)_4$ with some experimental values (Neck et al. 2003; Moon 1989). The speciation of Th in Figure 4-2 illustrates Th speciation in the simplified groundwater used in our dissolution experiment.

In 0.1 M NaCl, $Th(OH)_4$ and the other hydroxide species are the prevailing species. In 0.01 M NaCl with 2mM $NaHCO_3$, the carbonate and mixed carbonate/hydroxides complexes are present.

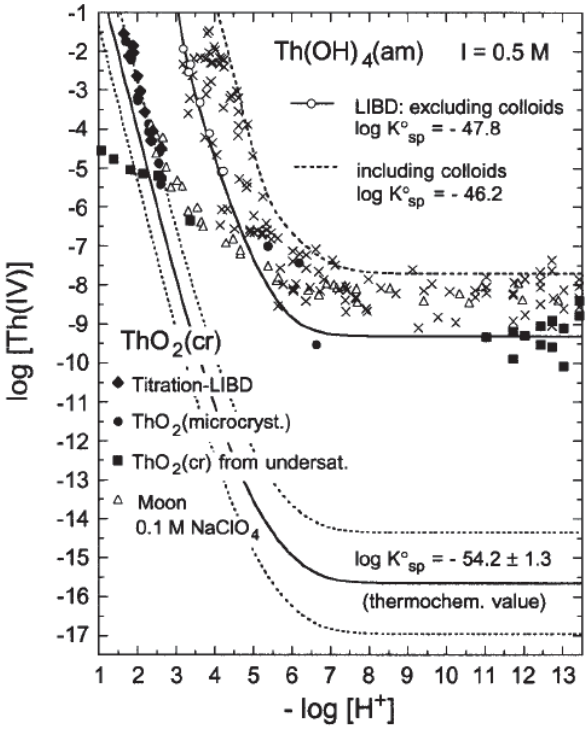

Figure 4-1. *Experimental and calculated solubility of ThO_2 (cr) and $Th(OH)_4$(am) at I = 0.5 M and 25 °C. The solubility data for ThO_2(cr) determined in (Neck et al. 2003) are presented with filled symbols from under and oversaturation and by LIBD- titration in 0.5 M NaCl and by Moon (1989) in 0.1 M NaClO4 at 18 °C (open triangles). The lines are calculated for I=0.5 M with the hydrolysis constants log $K°_{sp}(ThO_2(cr))$ = -54.2±1.3 and log $K°_{sp}(Th(OH)_4(am))$ = -47.0±0.*

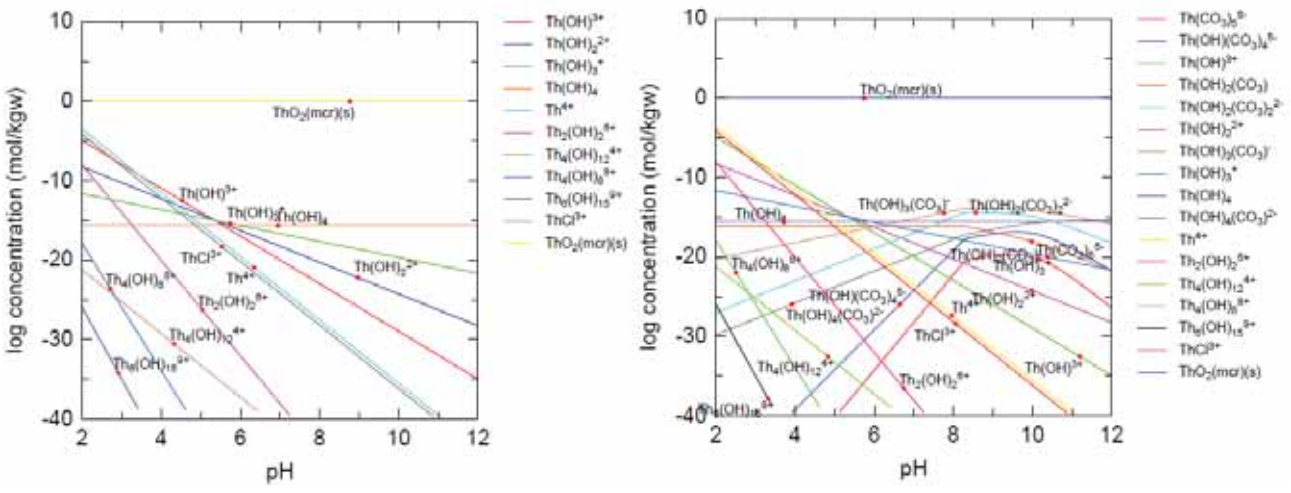

Figure 4-2. *Thorium speciation in 0.1 M NaCl and in 0.01 M NaCl (2mM $NaHCO_3$). Modelled with PHREEQC by using Andra's database Thermochimie7b.*

4.2 Experimental methods

The aim of the first year of the project was to conduct pre-tests for ThO_2 dissolution and define the research plan for the main experiments. The pre-tests were conducted with two different particle sizes in 0.1 M NaCl and 0.01 M NaCl (with 2 mM $NaHCO_3$) solutions under atmospheric conditions. Two particle sizes 10 to 40 µm and 2 to 4 mm were selected based on the previous experiments. The smaller 10 to 40 µm size particles has been used in the ThO_2 solubility studies (Hubert et al. 2001, Fourest et al 2000) and the bigger 2 to 4 mm particles in the UO_2 solubility tests (Ollila 2008a).

The sintered ThO_2 pellets used in the experiments were prepared as a part of WP1 in Sheffield to obtain ideal composition and microstructure similar to UO_2 fuel (Forsyth, 1987 and Forsyth, 1995). Thorium dioxide pellets were sintered from ThO_2 powder. The methodology was similar to the one described for CeO_2 in Chapter 2.2; it is described in detail in REDUPP Deliverable 1.1 (found on the REDUPP web page, www.skb.se/REDUPP). The optimized sintering temperature was 1750 °C, in which the density of prepared ThO_2 pellets was 93 % of the theoretical density. ThO_2 pellet surface topography and crystal orientation were analysed with confocal profilometry and EBSD at Stockholm University. The ThO_2 pellet samples were polished down to a 1µm finish using diamond paste and mechano-chemically etching in colloidal silica. The surface topography of polished sample was studied with a Sensofar PLu2300 confocal profilometer. ESEM /EBSD images of the sample were taken using a Philips (XL-30) field emission gun environmental electron microscope (FEG-ESEM) with coupled electron back scatter diffraction (EBSD) using the Oxford Instruments software package HKL Channel 5.

The sintered white pellets used for the dissolution experiments had an orange surface coloration. For the experiments, these pellets were crushed to pieces in mortar and the suitable size particles from 2 to 4 mm were selected for washing. The crushed material was treated by washing in isopropanol followed by gravitational settling in an attempt to remove adhering fine fragments. This was not successful, so the particles (Figure 4-3) were soaked one at a time on isopropanol followed by ethanol and then dried in a desiccators.

The rest of the material was ground in a ball mill (Retsch, MM2) to finer powder. The objective was to collect the fraction of particles from 10 to 40 µm by sieving after grinding.

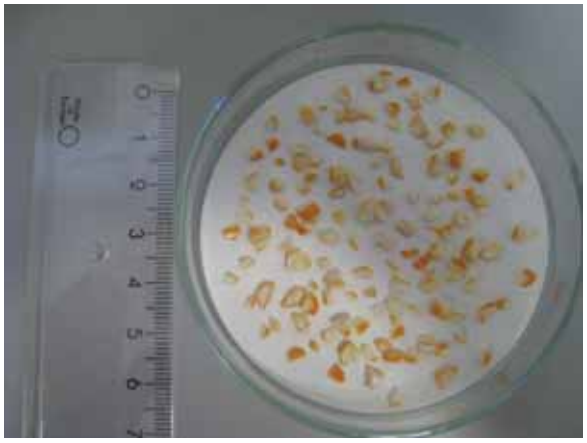

Figure 4-3. *Orange surface 2 to 4 mm ThO_2 particles after crushing and flushing with isopropanol and ethanol.*

Approximately 300 mg of 2 to 4 mm sized ThO_2 particles were weighed into each polypropylene vessel (50 ml). The vessel was filled with 50 ml of the simplified groundwater, either 0.1 M NaCl or 0.01 M NaCl (2mM $NaHCO_3$). In the case of smaller particle size, only 150 mg of ThO_2 powder (10 to 4 μm) was used in an otherwise similar test. Each test had one blank test without solid ThO_2 and two parallel tests with similar amount of solid ThO_2.

Sampling was conducted at 0, 1, 3, 6, 15, 24 and 31 days by withdrawing a 2.5 ml sample. Samples were ultrafiltered with a Pall Mall filtration device with 10 kD (~1 nm) molecular cut off by using centrifugation (6000 rpm, 1 h). In addition, some samples without filtration were also taken. Prior to sampling the test vessels with smaller 10 to 40 μm particles were centrifuged with Beackman & Coulter Avanti J-26 XPI Centrifuge (1 h, 5000 rpm ~ 4032 G) to prevent the take up of fine particles during the sampling.

All samples were acidified with s.p. HNO_3 (OPTIMA by Fisher Scientific) after filtration. Thorium concentrations were analysed with Element 2, high resolution inductively coupled plasma mass spectrometer (HR-ICP-MS).

Detection limits down to 10^{-15} mol/L should be achievable with Element 2 according to instrument manufacturer. So far, the level of 10^{-12} mol/L has been achieved, which is still much better compared to the detection limits achievable with the sensitivity of traditional quadrupole ICP-MS.

4.3 Preliminary Results

The surface analyses showed the presence of randomly oriented crystals with grain size from 10 to 30 μm (see Figure 4-4).

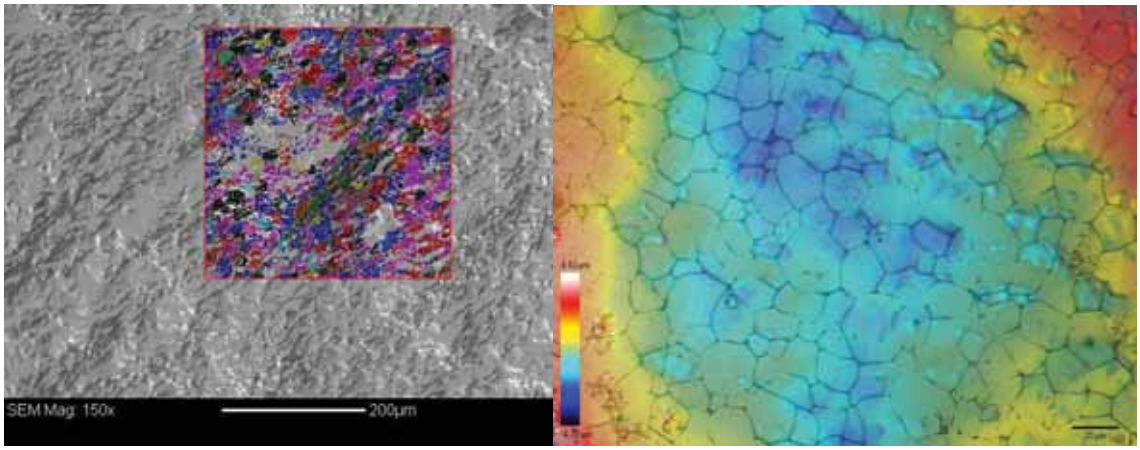

Figure 4-4. *EBSD map and profilometer image of the polished top surface of the ThO_2 pellet.*

In the batch tests with larger particles (2 to 4 mm), the thorium concentration of ultrafiltrated samples showed increasing trend as function of time in both test solutions (see Figure 4-5). The Th concentration of unfiltered samples increased more rapidly to higher level and then decreased slowly. The difference between filtered and unfiltered samples was clear in the beginning of the test. Also the effect of carbonate complexation to solubility was observed, as the 0.01 M NaCl solution with 2 mM of $NaHCO_3$ had higher concentrations of Th compared to concentrations in the 0.1 M NaCl. However, the results in 0.01 M NaCl solution with 2 mM of $NaHCO_3$ and in 0.1 M NaCl are not directly comparable due to the difference in pH. The pH also has some effect on solubility as was illustrated in Figure 4-1.

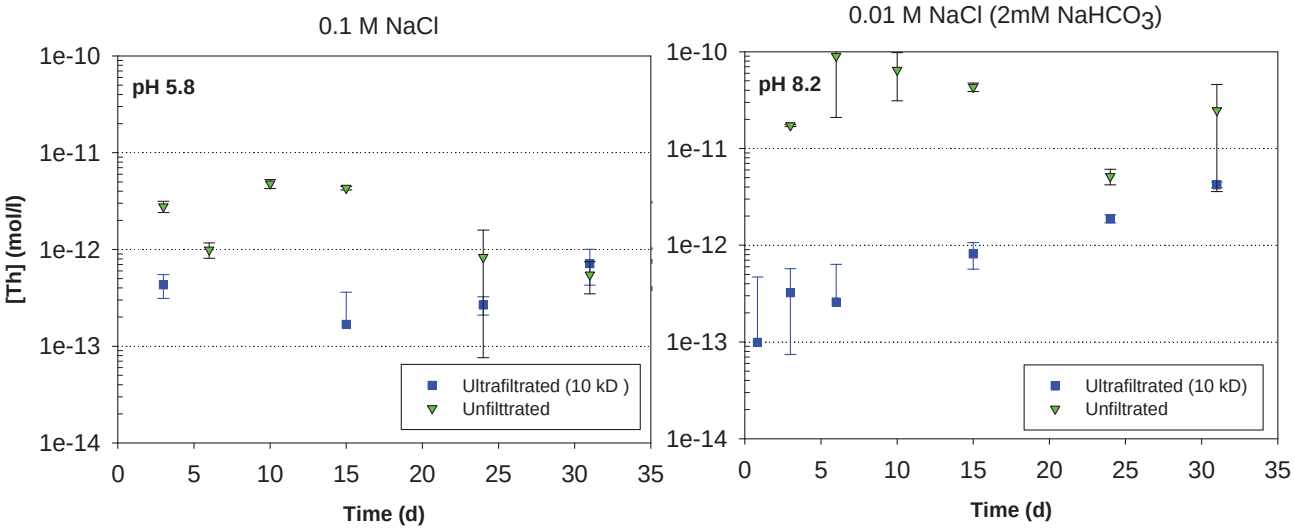

Figure 4-5. *The evolution of Th-232 concentration in batch tests conducted with 2 to 4 mm particles.*

4.4 Summary and future work

The microstructure of the sintered ThO_2 was similar to UO_2. In dissolution batch tests the concentrations of Th were measurable. The presence of hydroxide species/colloids was observed as a difference in concentrations between the unfiltered and ultrafiltered samples. The solubility increasing effect of carbonate complexation was also observed as when test solution with and without $NaHCO_3$ were compared. In the future, the purity of ground ThO_2 powders will be tested, for example with XRD, before starting actual tests with smaller particle sizes. XPS or SIMS technique could be used to determine the origin of orange colour on the surface of the ThO_2 pellets. The artificial isotope ^{229}Th could be used to study if the dissolution/ precipitation phenomena occur during the dissolution. The ^{229}Th tracer could also help to avoid the problems with the detection limit of HR-ICP-MS, which is close to the solubility of ThO_2 in basic conditions. Instead the concentrations of ^{229}Th and ^{232}Th could be measured with alpha spectroscopic methods. Immobilized and polished ThO_2 fragments are planned to be prepared to follow the evolution of the surface as a function of reaction time with profilometry and EBSD.

5 DISSOLUTION OF UO_2 IN NATURAL GROUNDWATER (WP 4)

By Kaija Ollila, VTT

5.1 Introduction

In the safety case, release of radioactivity from the geological repository is controlled by the dissolution of the spent fuel in groundwater. Groundwater will come into contact with the spent fuel when the disposal container eventually fails. The fuel will be protected from contact with water by a corrosion resistant copper canister with a massive cast-iron insert and by a bentonite buffer. In the case of a potential canister defect and groundwater intrusion, the iron will react with water to produce Fe^{2+} and dissolved hydrogen under the prevailing anoxic conditions. The reducing conditions near the fuel surface may be altered only as a result of the radiolysis of the groundwater by ionizing radiation associated with the fuel. The nature of the radiation field changes with time. Young spent fuel has a radiation field that is dominated by β- and γ-decays. However, after a few hundred years, spent fuel will be less radioactive and α-decays will dominate the radiation field. The α-activity persists over much longer time periods and must therefore be taken into account.

The influence of alpha radiolysis on the dissolution behaviour of old spent fuel has been studied using substitute materials, such as UO_2 pellets that contain isotopes of U with relatively short half-lives. In this study, UO_2 doped with 0, 5 or 10 % ^{233}U is used to simulate the degree of α-radiation that will be present in spent fuel at various times after disposal. 5 and 10 % ^{233}U-doped UO_2 simulate the alpha activity of spent fuel 10 000 and 3 000 years after disposal, respectively (Ollila et al. 2004). Dissolution tests with this UO_2 material have been conducted previously in the In Can Processes and in the Near Field Processes projects supported by the European Commission under the 5th and 6th Framework Programs (Ollila et al. 2004; Ollila 2008b). Until now, tests have been conducted in synthetic groundwaters under actively reducing conditions at ambient glove box temperature. Synthetic groundwaters have included modified Allard groundwater, which simulated fresh groundwater conditions (Vuorinen & Snellman 1998) and 0.01 M – 1 M NaCl solutions (Ollila 2008b). The measured dissolution rates varied from 2×10^{-8} to 1×10^{-7} fraction/yr, see Table 5-1. There was no indication of an effect of alpha radiolysis on the dissolution rate results of the samples with doping levels of 0, 5 and 10 % ^{233}U. The increase in the ionic strength seemed to have a decreasing effect on dissolution rate. Generally, these UO_2 solid samples have experienced many years of dissolution time and showed dissolution rates that were slowly decreasing with each subsequent exposure to synthetic groundwater. This suggests the disappearance of the high energy sites such as sharp edges and defects generated by the crushing process.

However, the synthetic groundwaters used do not contain all of the chemical elements that occur in natural groundwaters. Some of the trace elements may produce aggressive radiolysis products or cancel out the effects of H_2 (e.g. Br^-, Metz et al. 2008). This could increase the dissolution rate of spent fuel. The objective of Work Package 4 is to determine whether the presence of trace elements in natural groundwaters affects the

dissolution rate of UO_2 in the presence of alpha radiation. Another objective is to study the effects of secondary phase formation and/or surface reconstruction by loss of high energy surface sites. Three natural groundwaters are chosen for the tests with ^{233}U-doped UO_2 samples. These will include a low ionic strength groundwater, a moderately saline groundwater, and a high salinity water. This report gives preliminary results obtained in dissolution experiments in the first natural groundwater.

Table 5-1. *Dissolution rates of U (mol m^{-2} yr^{-1}) in synthetic groundwaters in the presence of corroding iron (Ollila & Oversby 2005; Ollila 2008b). Values in parenthesis are fractional dissolution rates (fraction/yr) based on mass of U.*

UO_2 solid doping level	0.01 M NaCl	0.5 M NaCl	1 M NaCl	modified synthetic groundwater (Allard)
0 % ^{233}U (1)	2.1 x 10^{-6} ($1x10^{-7}$)	2.7 x 10^{-6} ($1x10^{-7}$)	6 x 10^{-7} ($3x10^{-8}$)	2.7 x 10^{-6} ($1x10^{-7}$)
0 % ^{233}U (2)	4.2 x 10^{-6} ($2x10^{-7}$)	2.5 x 10^{-6} ($1x10^{-7}$)	1.1 x 10^{-6} ($5x10^{-8}$)	2.9 x 10^{-6} ($1x10^{-7}$)
5 % ^{233}U (1)	2.1 x 10^{-6} ($1x10^{-7}$)	2.3 x 10^{-6} ($1x10^{-7}$)	4 x 10^{-7} ($2x10^{-8}$)	2.1 x 10^{-6} ($1x10^{-7}$)
5 % ^{233}U (2)	8 x 10^{-7} ($4x10^{-8}$)	1.2 x 10^{-6} ($5x10^{-8}$)	6 x 10^{-7} ($3x10^{-8}$)	2.7 x 10^{-6} ($1x10^{-7}$)
10 % ^{233}U (1)	8 x 10^{-7} ($4x10^{-8}$)	1.3 x 10^{-6} ($6x10^{-8}$)	4 x 10^{-7} ($2x10^{-8}$)	2.7 x 10^{-6} ($1x10^{-7}$)
10 % ^{233}U (2)	8 x 10^{-7} ($4x10^{-8}$)	1.3 x 10^{-6} ($6x10^{-8}$)	4 x 10^{-7} ($2x10^{-8}$)	2.7 x 10^{-6} ($1x10^{-7}$)

5.2 Natural groundwater

The first natural groundwater chosen for the dissolution tests was a brackish groundwater from Olkiluoto site from the depth of 135 to 137 metres (borehole KR6/135/8). It is a moderately saline groundwater (TDS 6300 mg/l) with slightly alkaline pH 7.7. Total alkalinity is 2.3 mmol/l. The water has high Na (1560 mg/l), Ca (510 mg/l), Mg (150 mg/l), Cl (3440 mg/l) and SO4 (419 mg/l) contents. The content of Br is 12 mg/l. The content of iron is 0.35 mg/l.

Five litres of OL-KR6 groundwater was sampled to 10 glass bottles (500 ml) from the borehole in Olkiluoto and transferred to VTT in Otaniemi. The bottles were transferred to Ar atmosphere and the water samples were poured in four Nalgene bottles made of high density polyethylene (1.5, 1.5, 1.5 and 0.5 litres). The measurements with Orbisphere Analyser showed that the waters had some oxygen (ca. 1 ppb). All the groundwater samples were purged with Ar to remove this residual oxygen. After this, the analyser showed the oxygen level to be 0.01 to 0.02 ppb. The CO_2 content was not measured.

Subsequently, the groundwater samples were allowed to stay in Ar atmosphere and the stability of the water in Ar atmosphere was followed doing pH measurements and alkalinity titrations at suitable intervals, see Figure 5-1. The purpose was to equilibrate the waters prior to the start of the dissolution tests. The groundwater samples apparently lost carbon dioxide when they were purged with Ar. Hence, the pH of the water increased from 7.7 to 8.6 and the bicarbonate content decreased from 140 ppm to 50

ppm. The total alkalinity (HCl uptake) decreased from 2.30 to 0.70 mmol/l. After 100 days, both ph and the bicarbonate content seemed to stabilize. The analysis of water composition was performed after 100 days from the transfer of the water samples. Microfiltered and (0.22 µm) and nonfiltered samples were analysed.

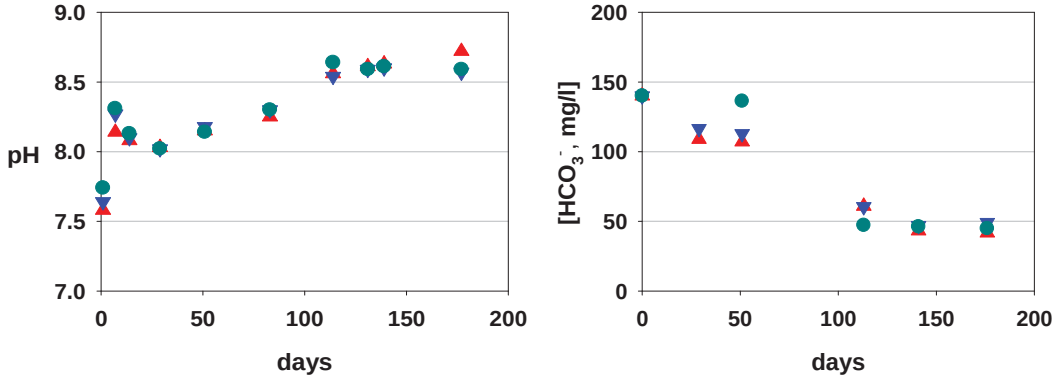

Figure 5-1*. pH and [HCO_3^-] for OL-KR6 groundwater samples during 175 days' period after the transfer of the samples to the Ar atmosphere of the glove box. The data is for three groundwater samples (1.5 litres each).*

The results did not suggest the presence of precipitations. Similar results were obtained for the main cations (Na^+, Ca^{2+}, Mg^{2+}, K^+, Si^{4+}, S_{tot}, Fe_{tot}) and anions (Cl^-, SO_4^{2-} and Br^-) in the samples with or without filtration. The content of total iron (0.15 mg/l) had decreased from the original value (0.35 mg/l).

5.3 Experimental methods

The dissolution rates were determined using the isotope dilution technique to decrease uncertainties due to precipitation effects. This technique can be used to determine whether a solid in contact with solution is continuing to dissolve and reprecipitate even though the solution concentration is constant or even decreasing. The dissolution test of a solid UO_2 sample is started in a spiked solution that has a U content close to that expected at equilibrium or steady state, but a $^{235}U/^{238}U$ isotopic ratio far from that of the solid UO_2. By measuring the [^{238}U] and the ratio of $^{235}U/^{238}U$ in the solution sample we can calculate whether there is U being added to solution from the solid phase. Even if precipitation or sorption occurs, the change in isotopic ratio will give the amount of the material processed through solution. The detailed description of the method is given elsewhere (Ollila et al. 2004; Ollila 2008b). In the dissolution tests of this study, a standard reference material, U_3O_8 (s), with a $^{235}U/^{238}U$ ratio of 10.354 ± 0.758 was used as spike. The U_3O_8 was dissolved in 1 M HNO_3. The spike solution was deaerated and stored in the glove box. The oxidation state of U in the spike was U(VI).

The solid UO_2 samples and their isotopic compositions are given in Table 5-2. UO_2 samples are as UO_2 fragments of the size range 1.4 to 4 mm. The UO_2 fragments doped with ^{233}U were produced by BNFL (British Nuclear Fuel Limited).

Otherwise the method of the dissolution experiments was a static batch dissolution procedure (Ollila 2008b). The water phase (OL-KR6 groundwater) was allowed to stay with an iron strip in solution for two weeks prior to the start of the experiments. Subsequently, the water phase was filtered (0.22 μm).

Table 5-2. *The solid UO_2 samples.*

UO_2 sample	[^{233}U] (%)	[^{235}U] (%)	[^{238}U] (%)	^{235}U/^{238}U	(g)
Undoped	0	2.82	97.18	0.029	1, 1, 3
5% ^{233}U-doped (15.7 MBq/g)	5.0	4.5	90.5	0.050	1, 1, 3
10% ^{233}U-doped (31.4 MBq/g)	10.0	4.5	85.5	0.053	1, 1, 2.5

The solid UO_2 sample (1 g or 3 g fragments) was placed on a fused silica 'saucer', which was immersed in Fe-equilibrated OL-KR6 groundwater (40 ml) in a vessel made of polypropylene. A new iron strip was added. After this, an aliquot of spike solution was added. The total [U] addition was 0.8 ppb (3 x 10-9 mol/l, 235U/238U= 10.354). The test vessels were closed and placed in an additional vessel to protect from the effects of trace oxygen in the atmosphere of the glove box. The samplings were made 2 hours after the spike addition and at the intervals of 1 to 2 weeks thereafter.

5.4 Preliminary results and discussion

The measured ^{238}U concentrations for the first test series with the ^{233}U-doped UO_2 samples (1 g fragments) in OL-KR6 groundwater are given in Figure 5-2 (on the left). The right-hand Figure gives the total U concentrations including the ^{235}U from the spike. The U concentration decreases strongly during the first 20 days. The amount of the added spike is relatively high under these strongly reducing conditions controlled by iron leading to the precipitation of uranium. Afterwards, the U concentration seems to level off or is slowly decreasing. There is no difference between different doping levels. The test time is relatively short so far. The measured U concentration in solution in the 67 days' samples was (2.98 ± 0.69) x 10^{-11} mol/l. Table 5-3 shows the measured U concentrations in the 67 days'samples in nanograms/l. The analyses were performed with High Resolution ICP-MS which has a low enough limit of quantification. The relative standard deviations of the measurements varied from 11 to 28 %. The samples were diluted in the ratio of 1 to 6 before measurements due to the salinity of the groundwater.

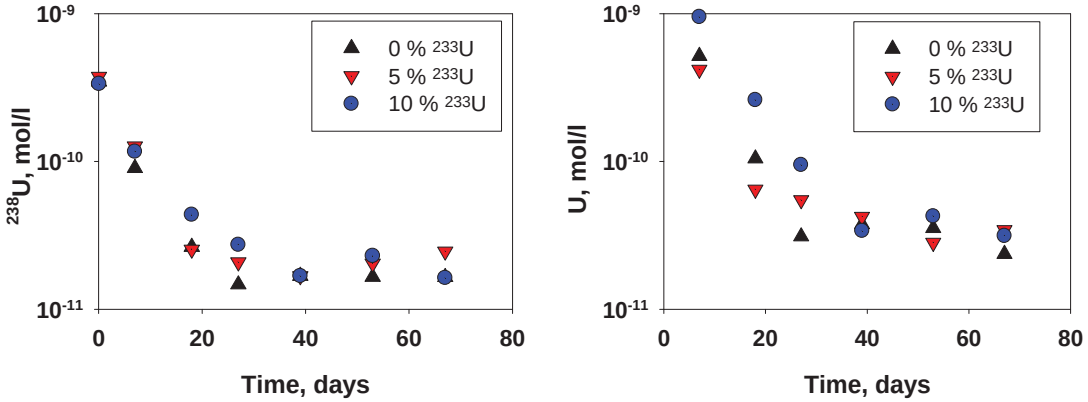

***Figure 5-2**. Measured [^{238}U] (on the left) and [total U] ($^{235}U+^{238}U$) (on the right) in OL-KR6 groundwater under reducing conditions produced by corroding Fe. The data are average values of parallel tests for each doping level (0, 5, 10 % ^{233}U).*

***Table 5-3**. Measured ^{238}U concentrations in OL-KR6 natural groundwater after 67 days' test duration. The analyses were performed with High Resolution ICP-MS.*

UO_2 sample	^{238}U (ng/l)	Relative standard deviation (%)
0 % ^{233}U (1)	5.1	28
0 % ^{233}U (2)	2.8	11
5 % ^{233}U (1)	2.9	17
5 % ^{233}U (2)	8.8	14
10 % ^{233}U (1)	4.6	26
10 % ^{233}U (2)	3.1	16

The U concentration in the solution is lower than the solubility limit of amorphous UO_2, $10^{-8.5}$ to $10^{-9.5}$ M (given by Fors et al. 2009). The calculated solubility for a crystalline solid, UO_2 (c), 1.45 x 10^{-15} M, is many orders of magnitude lower.

The preliminary results in natural OL-KR6 groundwater are in agreement with previous results in simulated groundwater, see Figure 5-3. The ^{238}U concentrations calculated from the changes in the measured $^{235}U/^{238}U$ ratios are higher. The calculated [^{238}U] may represent colloidal U or U present as complex ions. The calculated ^{238}U concentration increases slowly. More data is needed for calculating dissolution rates. The measured ^{238}U concentrations in natural groundwater are lower than in 0.01 M NaCl solution. The reason for this may be the more sensitive analytical method (HR-ICP-MS). The analyses in previous studies were performed with conventional ICP-MS and the ^{238}U concentrations were close to the detection limit. The calculated ^{238}U concentrations at the different doping levels are given vs. time in Figure 5-4. There is scatter in the results. No clear difference can be seen between the doping levels. The calculated [^{238}U] increases to the end of the experimental time so far (67 days).

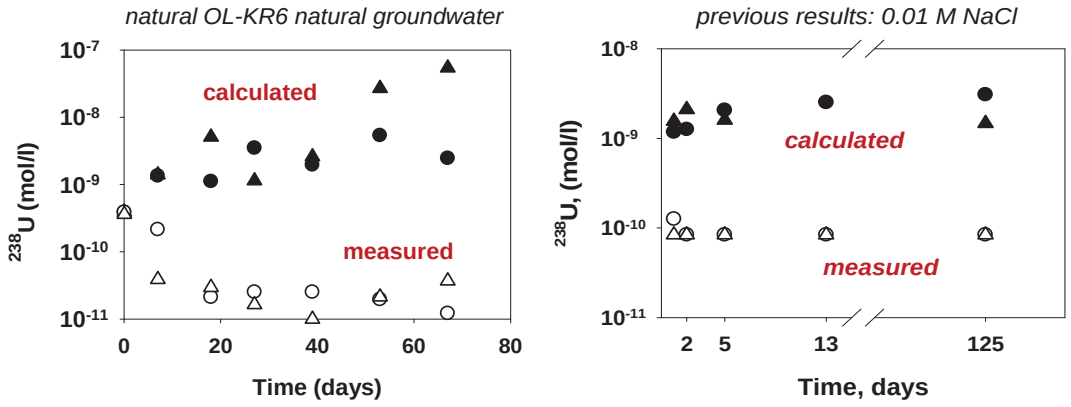

***Figure 5-3**. Measured [^{238}U] and [^{238}U] calculated from the isotopic ratio changes in OL-KR6 groundwater and in 0.01 M NaCl solution (SA/V= 5 m^{-1}) under reducing conditions (Fe). The results are data for parallel isotope dilution tests with 5 % ^{233}U-doped UO_2 fragments.*

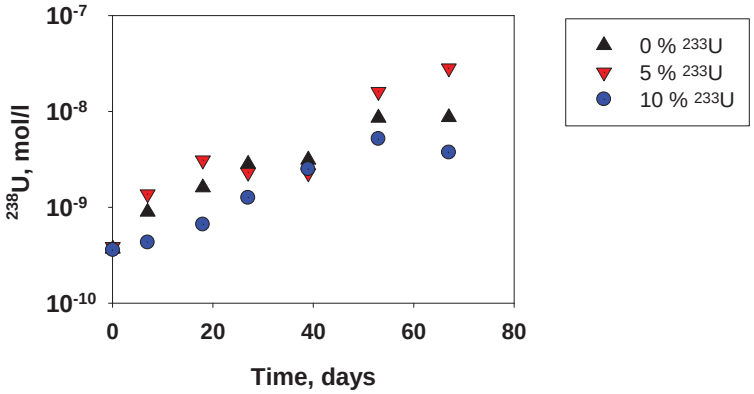

***Figure 5-4**. Calculated [^{238}U] vs. the doping level of the solid UO_2 in OL-KR6 groundwater under reducing conditions. The data are average values of parallel tests for each doping level (0, 5, 10 % ^{233}U).*

5.5 Summary and future work

Preliminary results of the isotope dilution experiments with 0, 5 and 10 % ^{233}U-doped UO_2 samples in OL-KR6 natural groundwater (SA/V= 5 m^{-1}) under reducing conditions with iron are in agreement with the previous results of the tests in simulated groundwater. They do not suggest any effects of alpha radiolysis on dissolution. A new series of tests using a higher SA/V (15 m^{-1}) has been started. The results for the first month show higher release of U from 10 % ^{233}U-doped UO_2 sample, compared with the lower doping levels.

Previous studies with undoped and and alpha-doped UO_2 suggest the precipitation of secondary phases in the presence of corroding iron. Dissolution experiments with Gd_2O_3 doped UO_2 using a high SA/V and long duration will be started. The aqueous phase is a synthetic groundwater. The composition of the water for glove box conditions

(Ar) is planned by equilibrium modelling (PHREEQE or EQ3NR). The reference water is the brackish OL-KR6 or saline OL-KR20 Olkiluoto groundwater.

5.6 Acknowledgements

The author takes pleasure in thanking Maija Lipponen, Emmi Myllykylä and Jaana Rantanen for performing the HR-ICP-MS analyses.

6 SURFACE CHANGES DURING DISSOLUTION OF CeO_2 MONOLITHS (WP5)

By Claire L. Corkhill, Daniel J. Bailey and Neil C. Hyatt
University of Sheffield.

6.1 Introduction

In spent nuclear fuel, high energy sites occur at grain boundaries and within the material as naturally occurring surface defects (Shoesmith 2000). Current studies of spent nuclear fuel dissolution have not considered in detail the effect of high energy surface sites within the material structure. To complement the batch experiments using powdered CeO_2 (discussed in Chapter 3), the dissolution of monoliths of CeO_2 is described. These samples were monitored for the evolution of high energy sites, including pores, steps and dissolution pits. Preliminary results are discussed, which will form the basis for future investigation.

6.2 Experimental methodology

Monolith experiments were conducted using pressed and polished (0.05 μm, diamond paste) CeO_2 pellets (prepared as described in Chapter 2). The pellets were placed within pre-cleaned (ASTM C 1285-02) cold-sealed Teflon reactors (3 cm^3) on a spacer to ensure fluid contact all around the pellet. 2 ml 2M HCl was added to the vessel prior to closure. Reaction vessels were placed in an aluminium heating block, and heated to either 90 °C or 150 °C. Samples were removed at 1, 3, 7, 14 and 21 days for imaging by Scanning Electron Microscopy (SEM) and Optical Profilometry. The reaction fluid was also removed at these time periods and analysed for Ce concentration by ICP-MS. This was replaced with fresh reaction solution

6.3 Preliminary Results

Figure 6-1 shows the extent of CeO_2 dissolution at 150 °C after 9 and 21 days. After 9 days (Figure 1b), it is clear that the grain boundaries have undergone extensive dissolution compared to the pristine sample (Figure 1a), etch pits have formed in some of the grain surfaces (mostly triangular in shape), and some grains appear to have dissolved more than others, as shown by the height contrast between grains. After 21 days (Figure 1c and d), the surface of the sample has been severely transformed, with no observable grain boundaries. It is also clear that triangular facets are present on the surface of the least dissolved grains (Figure 1d, insert).

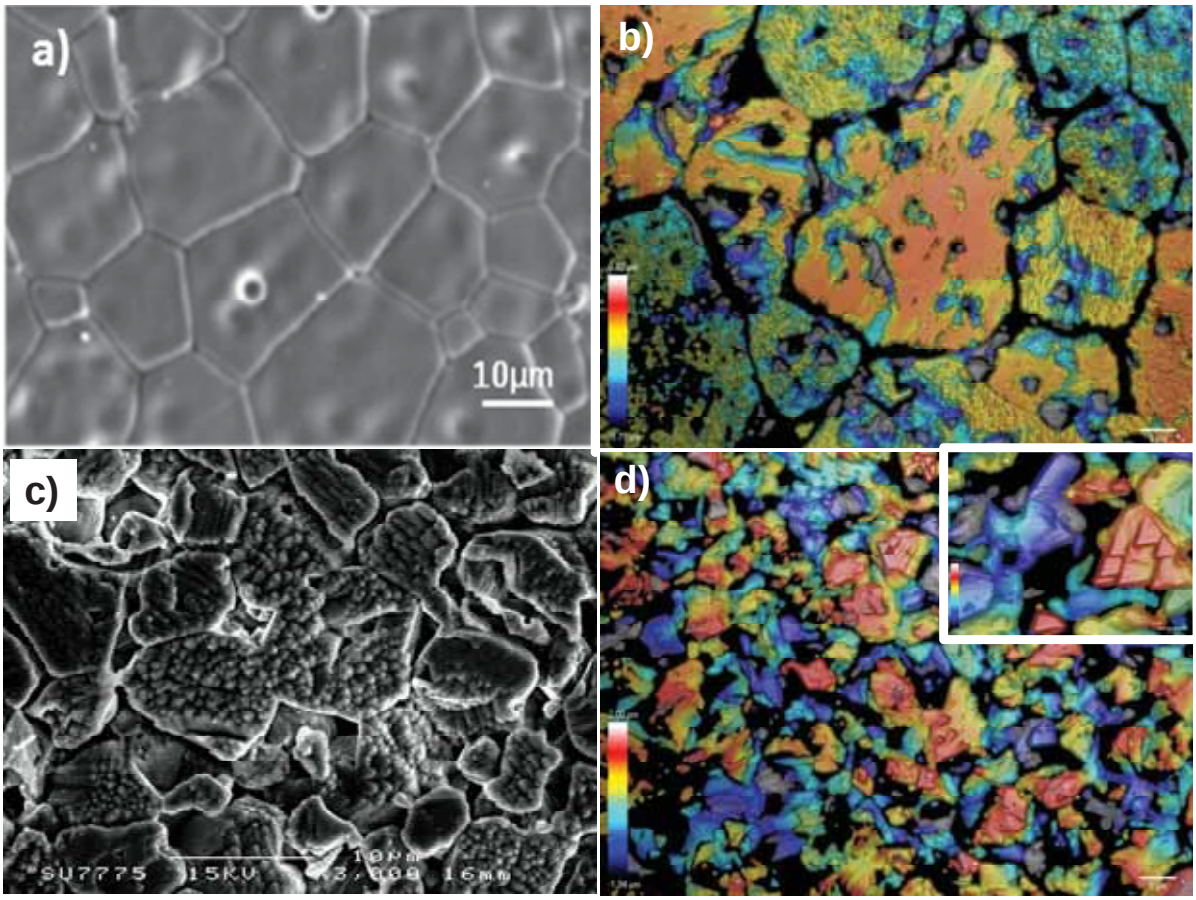

Figure 6-1. *SEM and confocal profilometer images of CeO_2 monolith samples a) pristine, b) after 9 days reaction in 2M HCl at 150 °C , and c) and d) after 21 days reaction in 2M HCl at 150 °C. Insert in d) shows a x 4 magnified area of image in d).*

For CeO_2 reacted at 90 °C under identical conditions, relatively little change was observed at the sample surface. This is evident in the leached Ce concentration date for CeO_2 leached at 90 °C compared to 150 °C, as shown in Figure 6-2. Dissolution at both temperatures show a linear trend, but for dissolution at 150 °C, the concentration of Ce is an order of magnitude higher than that for 90 °C, giving concentrations after 14 days reaction of 83.3 ppm and 8.3 ppm, respectively.

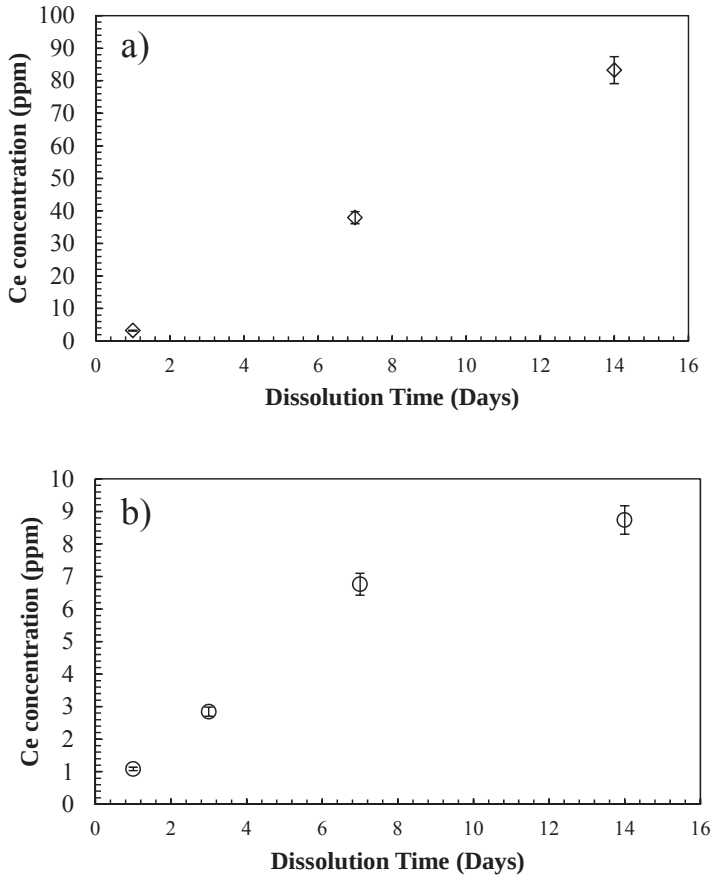

Figure 6-2*. Concentration of Ce in solution resulting from CeO_2 monolith dissolution in 2M HCl at a) 150 °C and b) 90 °C. Error shown is instrument error of 5 %.*

6.4 Summary and future work

Results from this preliminary study indicate that several factors control the evolution of morphology of CeO_2 samples during dissolution. Preferential leaching of some grains and the presence of triangular facets suggest a crystallographic control on leaching. This is consistent with investigations on fluorite, which has the same crystal structure as CeO_2 (Godinho et al. 2012). Further work using electron backscatter diffraction has begun to elucidate this mechanism. Temperature has also been observed to control dissolution, with dissolution at 150 °C resulting in Ce concentrations in solution an order of magnitude higher than for 90 °C. Further work to carefully determine the thermodynamics of dissolution is also underway.

7 AB INITIO MODELING OF SURFACE DEVELOPMENT OF FLUORITE-TYPE SOLIDS (WP 6)

By Pablo Maldonado and Peter Oppeneer, Uppsala University

7.1 Introduction

The dissolution of UO_2 spent fuel is difficult to study under laboratory conditions, due to the restrictions in handling the radioactive material. However, chemical processes down to the atomic level can nowadays be ideally and accurately simulated using modern computational modeling techniques, such as the density-functional theory (Jones and Gunnarsson 1989). The objective of this Work Package (WP) is to perform first-principles materials modeling of nuclear-fuel surfaces to simulate the dissolution process. The tasks in this WP include computing how the surface of an irregularly shaped solid changes as the solid dissolves and how the shape of the surface in turn influences the dissolution.

As measurements on the surface structure of UO_2 spent fuel can only be done in specialized laboratories, detailed studies will be performed on several materials having the same fluorite structure as UO_2, namely, CeO_2, CaF_2, and ThO_2. Through studying these related fluorite materials we expect to be able to correlate the experimental data with results obtained from the first-principles materials modeling. Having thereby reached understanding for the dissolution of CeO_2, CaF_2 and ThO_2, first-principles results obtained for UO_2 will be extrapolated to describe the time-evolution of its dissolution process. As a second step to be undertaken later on, computer simulations of the chemical reactions likely to take place at fluorite surfaces will be carried out.

7.2 Main research directives and work undertaken in the first year

The following tasks have been performed in the first year:

1. setting-up the calculations for the bulk materials CaF_2, CeO_2, and UO_2
2. benchmarking these calculations against other calculations and experiments
3. setting-up the calculations for stepped surfaces, including high-index planes
4. computing the surface formation energies of these stepped surfaces
5. computing the defect formation energies of specific defects at the surfaces

The above calculations are directly connected to other tasks being performed within the consortium as well as in the related FP7 project Delta-Min ("Mechanisms of mineral replacements reactions"). The dissolution of high index surfaces of CaF_2 have recently been measured in this context, using 3D confocal profilometry (Godinho et al. 2012). This work shows that the dissolution of the surface, given by the retreat rate, depends clearly on the Miller index (h,k,l) characterizing the surface, see Figure 7-1 below. These results imply that certain stepped surfaces dissolve faster than other surfaces. The (111) surface is, for example, observed to be very resistive against dissolution.

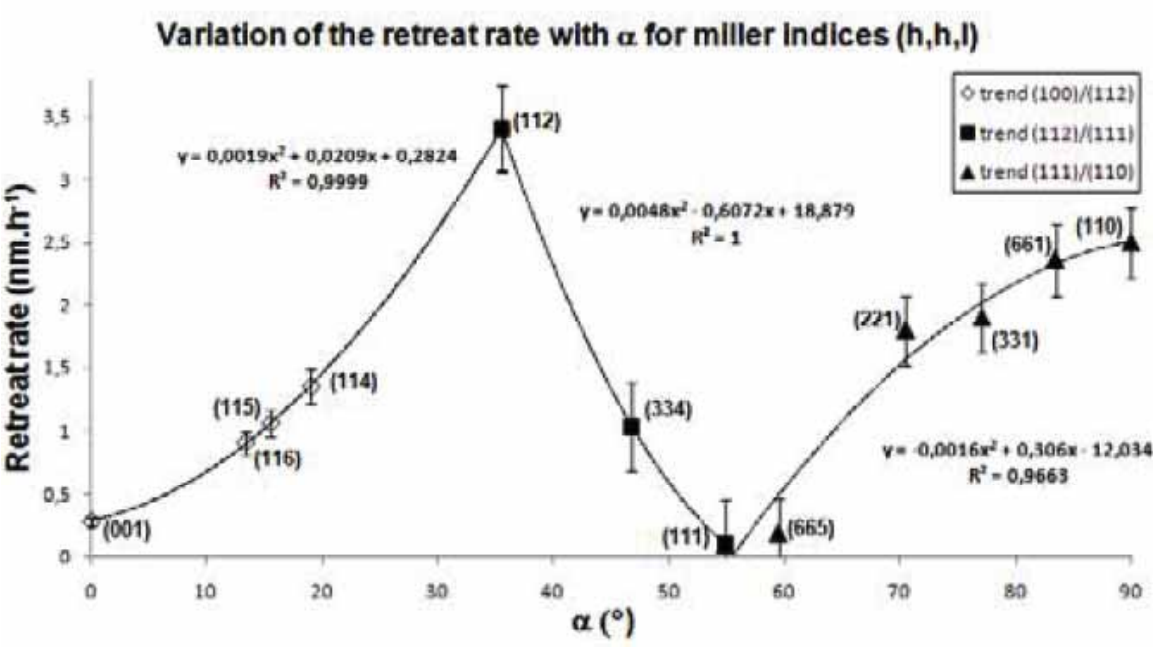

Figure 7-1*. The measured retreat rates in nm/hour for specified surfaces of CaF_2, indicated by their Miller indices (h,h,l). From Godinho (2011).*

To achieve an understanding of the particularities of the dissolution processes, these experimental data are to be complemented with data from first-principles calculations.

7.3 Computational methodology

The first-principles modeling calculations have been performed using the density functional theory (DFT) (see e.g. Jones and Gunnarsson 1989). In the DFT the exchange-correlation functional is an important ingredient and it needs to be properly chosen. In the calculations we have tested and used the following exchange-correlation functionals: the local density approximation (LDA), the generalized gradient approximation (GGA), as well as the corrected DFT+U approach, in which an additional Hubbard U parameter is introduced for the Ce 4f or U 5f electrons, to capture the strong on-site Coulomb interaction between f-electrons. This helps to remove so-called self-interaction effects and provides an improved description in particular for UO_2 (Yun and Oppeneer 2011; Yun et al. 2011).

The calculations have been performed with the Vienna Ab-initio Simulation Package (VASP), which is a plane-wave based electronic structure code. The electron-ionic core interaction on the valence electrons in the systems is represented by the projector-augmented wave potentials (PAW). For Ce and O atoms the (5s,5p,6s,4f,5d) and (2s,2p) states, respectively, were treated as valence states, while for Ca and F the 4s and (2s,2p) states were used as valence states.

Bulk fluorite crystals have the face centered cubic (fcc) structure. For the simulations also reciprocal space integrations are required, which were performed on a special k-point mesh generated by the Monkhorst-Pack scheme (9×9×9 in the bulk).

For all investigated surfaces the positions of the surface atoms have been optimized in the self-consistent electronic structure calculations by minimizing the Hellmann-Feynman forces acting on each atom until the total forces for each atom were smaller than 0.01 eV/Å.

The here-performed ab initio modeling calculations are computationally very demanding. Therefore there are not many groups that can presently perform such calculations. The work is carried out on various supercomputers in Sweden, to which the group at Uppsala University has good access (note that computer time is granted according to a ranking of competitive applications on a national level). Most of the calculations are carried out at the Cray supercomputer "Lindgren" at PDC Stockholm; a typical usage within WP6 is around 200 000 CPU hours per month. Nonetheless, the computational modeling is relatively low-cost compared to actual laboratory experiments.

7.4 Results of ab initio modelling

7.4.1 Benchmarking studies

To access the accuracy of the calculations and determine the parameters for proper convergence, a set of benchmarking studies has been performed. The benchmarking has been done separately for bulk fluorite crystals and for their surfaces.

The benchmarking calculations for bulk CaF_2 have been performed using the GGA exchange correlation potential (in so-called PBE parameterization), whereas the calculations for CeO_2 have been performed with the LDA+U exchange correlation functional (in the so-called Dudarev formulation), and the Coulomb U was taken to be 5.5 eV. Results of the benchmarking calculations for the bulk CaF_2 and CeO_2 materials are shown in Table 7-1.

Table 7-1. *Comparison between ab initio computed properties of CaF_2 and CeO_2 and available experimental data.*

	Comp. values	**Exp. Values**
CaF_2		
Optimized lattice parameter	5.516 Å	5.46 Å
Bulk modulus	80.84 GPa	82.71 GPa
Band gap insulator	7.38 eV	12.1 eV
CeO_2		
Optimized lattice parameter	5.401 Å	5.41 Å
Bulk modulus	212.45 GPa	204-236 GPa
Band gap insulator	2.18 eV	3 eV

The first-principles quantities obtained for CeO_2 are very close to the experimental values, implying that we have achieved an accurate description of its electronic structure. The results obtained for CaF_2 are slightly less in agreement. The optimized lattice parameter is larger than the experimental value (see Table 7-1), which is likely related to the GGA functional, which tends to overestimate the lattice parameter.

Once confidence in modeling the bulk electronic structure has been established, the next step is to benchmark the calculations for surface formation energies. Each surface plane in the cubic fluorite structure can be labeled by its Miller index, (h k l), denoting the crystal plane orthogonal to a vector (h k l) in the basis of the reciprocal lattice vectors. To determine the surface area for a certain (h k l) surface, a supercell slab is used, containing the surface plane, but also sufficient subsequent layers to describe the underlying material; an example is shown in Figure 2.

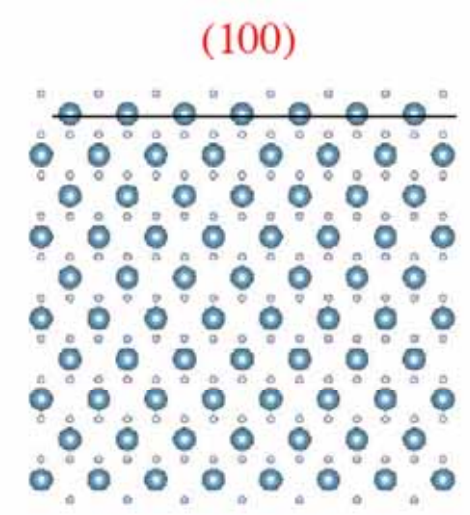

Figure 7-2*. Example of the modeling of the (100) surface. To represent the sub-surface material and to obtain an accurate value for the surface energy, sufficient layers below the surface need to be taken into account, as well as vacuum above the surface. Note that the (100) surface appears twice in the slab.*

The benchmark convergence with the number of layers, one considers the surface formation energy $E_{surf}^{(hkl)}$, for a general (h k l) surface, given by the quantity:

$$E_{surf}^{(hkl)} = \frac{(E_{slab} - nE_{bulk})}{2} \qquad (7\text{-}1)$$

where E_{slab} is the total energy computed for the slab system having a (h k l) indexed surface and E_{bulk} is the energy of the n-layers in the slab if there was no surface, i.e. the corresponding energy in the bulk system. Thus, the energy difference gives the energy that it costs to form the surface. The convergence of the surface energy with the number of layers in the simulation cell was tested (results are not shown here). The obtained surface energies compare reasonably well with older works, as is shown in Table 7-2. This table furthermore illustrates that an important aspect for obtaining proper surface energies is to relax completely all the atoms in the simulation cell; in some cases this

can lower the surface formation energy by 0.7 eV. One can also infer from Table 7-2 that the following order of surface stability is predicted: (111) > (331)> (110)> (211) > (100); i.e., the (111) surface is the most stable surface (consistent with the data in Figure 7-1).

Table 7-2. *Comparison of calculated surface formation energies (eV) of several surfaces of CeO2. Data in far right column are from this work, the rest are from Jiang et al (2005) and Skorodumova et al (2004).*

	HF	GGA(PBE)*	GGA(PW91)^	LDA^	LDA+U (This work)
Unrelaxed surface energy					
(111)	1.34	0.55	0.69	1.06	1.0275
(110)	2.61	1.09	1.26	1.55	1.6838
(100)		1.89	2.37		2.6845
(331)					1.5083
(211)					
Relaxed surface energy					
(111)	1.31	0.45	0.68	1.04	1.0164
(110)	2.11	0.86	1.05	1.35	1.4314
(100)		1.28	1.57		2.0092
(331)					1.2838
(211)					1.7383

* Jiang et al (2005), ^Skorodumova et al (2004)

7.4.2 Progress beyond benchmarking: Stepped surfaces

To approach the more realistic situation of an irregular surface, the surface formation energies of stepped surfaces have been computed. As an example, in Figure 7-3 the stepped (311) is shown. The immediate relation between studying such surfaces and the dissolution is the expectation that the atoms "sticking out from the surface" are those on the high-energy sites that are most easily to be removed.

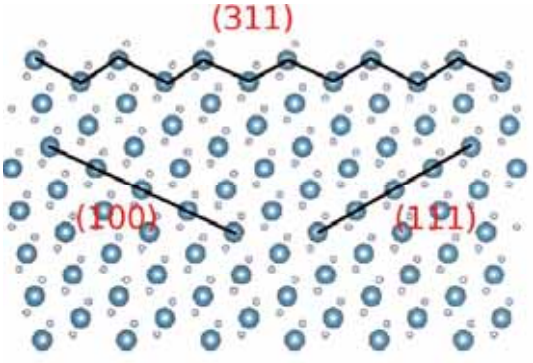

Figure 7-3*. Example of a stepped fluorite surface. The step on the (311) surface can be formed from two planes, the (100) and (111) planes.*

These calculations have been performed for CaF_2, one of the structural analogues for UO_2 (Godinho et al 2011). A similar procedure can be repeated for steps on other high-index planes; these can be constructed from a reference plane and a step in a second direction. Calculating the surface formation energies of such stepped surfaces can be quite time consuming.

As a result of the investigations, a very general relationship to describe the surface formation energy of stepped surfaces has been discovered. This relation can be expressed as

$$E^{(hkl)}(p) = (p - 1 + f)E^{ref} + \frac{\cos\alpha}{|\vec{A}|^2 |\vec{B}|^2} \qquad (7\text{-}2)$$

where $E^{(hkl)}$ is the surface formation energy of the stepped surface, E^{ref} that of the reference plane surface, p the number of rows, α is the angle defining the step, f a geometrical factor, and A and B are vectors defining the direction of the reference plane and the step direction, respectively. One example of such linear relation is shown below in Figure 4. The symbols in the left-hand panel give the ab initio calculated points, the line is the linear dependence. The definition of α and f is shown in the right hand panel for the stepped (511) surface. A consequence of the linear relation is that only a few energies of reference planes need to be computed, all other surface energies can be accurately estimated from the linear relation.

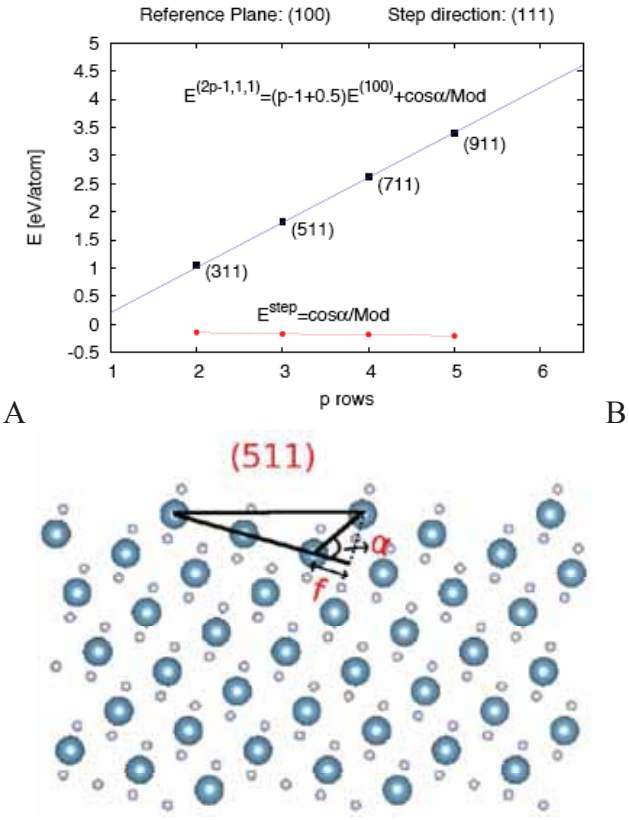

Figure 7-4. *General linear relation found for the surface energy of any stepped surface. A) ab initio computed data points compared to the linear relation. B) definition of the needed angle α and the factor f.*

7.4.3 Progress towards modeling dissolution process

The dissolution process has been investigated in two ways. One approach is to study the binding energies of atoms "sticking out" from the step edge. These calculations confirm that the atoms on the step edge have a small binding energy, i.e. they are most weakly bound. This work is currently continuing.

A second study, which has been undertaken recently, is that of the chemical reaction of molecules with the fluorite surface. In one of these studies the dissociation reaction of a H_2 molecule on the surface of (111) CeO_2 has been computed. The calculated energy barrier is shown in Figure 5. The H_2 molecule first weakly reacts with a Ce atom on the surface, maintaining the short distance typical for H_2. However, a small activation energy of about 0.1 eV is sufficient to lead to dissociation, in which the two H atoms separate and find each a minimum energy position on the surface. These calculations illustrate that calculating dissociation energies of other molecules such as H_2O should be possible.

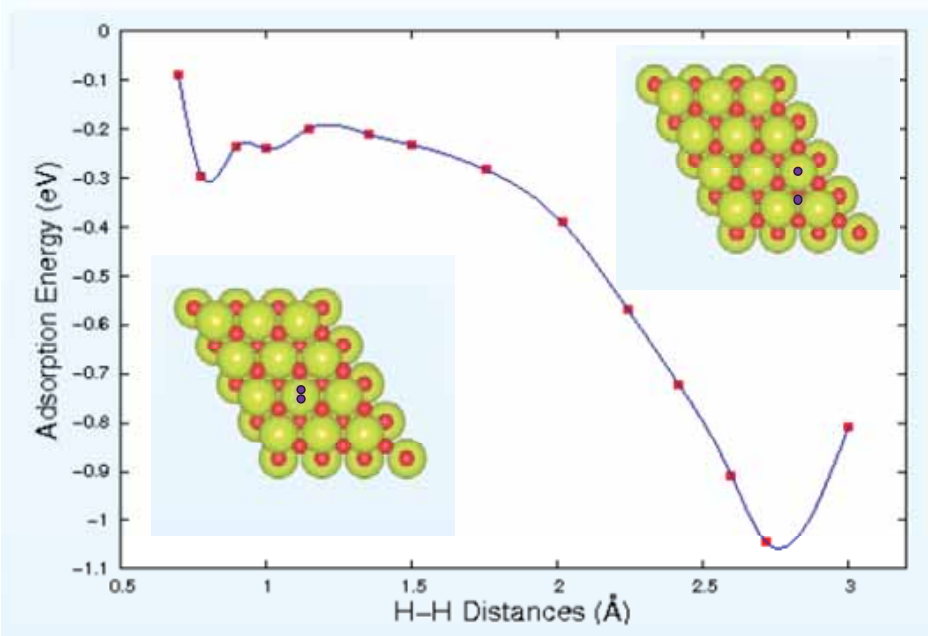

Figure 7-5. *Calculated reaction energy barrier of dissociative adsorption of H_2 on the CeO_2 (111) surface. A small energy (0.1 eV) suffices to overcome the barrier and induce dissociation of the H_2. The H atoms are the small darkly colored spheres, oxygen atoms the red spheres and Ce the yellow ones.*

8 COORDINATION AND MANAGEMENT (WP7 & WP8)

By L.Z. Evins, SKB

The Coordinator role involves many tasks, in particular to:

- Assure appropriate communication within the project,
- Compile & distribute periodic reports
- Supervise the implementation of the activities in the Description of Work
- Keep overall control of the project time schedule and resource plan
- Control compliance with project budget
- Control achievements of objectives with the stated time frames

The deliverables of WP7 and WP8 are planned in order to provide control over the management of the project and to make sure the planned work is running smoothly. Much of the efforts in these work packages are centred around the start and the reporting times of the project, but work is carried through continuously in order to keep communication going. An overview of the work performed and planned regarding coordination and management is given below.

8.1 The Project website

The project website was finished on time, within three months from Project start. It is found on the following address:
www.skb.se/REDUPP

It includes a Member Area which requires a Login which has been provided to the project participants. There are areas on the web site that require regular updating, for example News.

8.2 Communication Action Plan

The Communication Action Plan is posted on the web site. We are using the following Communication Tools:

- Participation in external conferences, meetings and workshops
- Scientific Publications
- Annual reports
- Web site (external and internal)
- Newsletter
- Professional magazines
- Press releases
- Internal: project meetings, emails, Member Area, etc

It can be noted that the project has already, after one year, used every tool listed (including press release; about research collaboration between the Sheffield and Japan).

8.3 Project presentation

The ‘Project presentation’ is a short text describing the project, required the by EC to use for communication concerning the project. This text is available on the REDUPP website, and the EC has used this text to put in a summary report of funded projects.

8.4 Meetings and workshops

The project participants plan to meet at regular intervals, both at the three planned Annual Meetings and at two more informal workshops. The First Annual meeting was held in Stockholm in April 2012, and this report presents a summary of the results so far. The other meetings are planned for April 2013 and the final meeting, which will be arranged as an open conference, is planned for February 2014.

Two Workshops were planned, and one has been held already at Stockholm University in September 2011. The aim was communication and initiation of collaboration. The next will be in September 2012; as mentioned below one or two lectures in the lecture Series are planned for this time.

8.5 Annual reports

There will be three Annual reports following the three Annual meetings. The present report is the first of this series, published and printed as a Posiva Working Report. The aim is that it will contain short reports from the on-going work in the different work packages. The audience is expected to be different Nuclear Waste Management Organisations, and the EC. The broader scientific audience will be reached through the peer-reviewed articles in scientific journals, which are a part of the project deliverables.

8.6 Annual newsletters

The Newsletter is planned for twice a year rather than once a year. The first REDUPP Newsletter was published after the first workshop in September 2011. It is posted on the EC website: http://cordis.europa.eu/fp7/euratom-fission/funded-reports_en.html

8.7 Lecture Series

The Lecture series is planned for 6-7 lectures with theme Surface reactivity/Surface processes during dissolution. The lecture series started in conjunction with the first Annual Meeting (26 April 2012) with Virginia Oversby’s lecture: “Spent fuel dissolution under repository conditions - why laboratory measurements always overestimate”. In all we had 15 project-external people attending the lecture and contributing to the discussions.

The rest of the lectures are planned for September 2012 and April 2013, and possibly one or two invited lectures during the final open conference.

9 SUMMARY

This report is the first annual report of the REDUPP project, which aims to investigate how surfaces of solids with a fluorite structure change with time during dissolution. In order to investigate how this may affect dissolution rate over time, laboratory experiments are performed to monitor dissolution, in connection with ab initio calculations. Another aspect of the project involves the effect of the complexity of natural groundwater on dissolution rate.

The goal is to develop a model of how the surfaces of fluorite-structures evolve during dissolution. This will reduce uncertainty regarding long-term spent fuel dissolution in a repository environment.

There are 6 research-based work packages, and three research teams. At Sheffield, the samples have been prepared and characterised (WP1), and the dissolution studies are focused around CeO_2 (WP2). The dissolution of the actinide oxides ThO_2 and UO_2 are studied at VTT (WP3 and WP4). During and after dissolution studies, the sample surfaces are analysed and characterised (WP5); this is done at Sheffield, VTT and at project-external laboratories, through collaboration. Ab initio modelling is performed at Uppsala university (WP6). The preliminary results after one project year were presented at the Annual Meeting and are documented here.

Sample material for further use in the dissolution studies have been prepared as pellets with similar microstructures as UO_2 (the exception is the UO_2 material used in WP 4, which was already available). The densities of the pellets were in excess of 96 % theoretical, and the microstructure consisted of equiaxed, randomly orientated grains in the size range between 5 μm and 20 μm.

Preliminary results of dissolution of CeO_2 powders show the expected trends for pH and temperature dissolution kinetics dependence. Further work will focus on using different sized crushed powders, giving different densities of high energy sites on the exposed surface, with the aim of achieving a detailed description of the evolution of surface morphology and the aqueous solution chemistry as dissolution occurs. The characteristics of CeO_2 monolith surfaces before and after dissolution were investigated using Scanning Electron Microscopy (SEM) and Optical Profilometry, and the preliminary results indicate that there is a crystallographic control on leaching, and that the grain boundaries are preferentially attacked.

Temperature was also observed to have a significant effect on dissolution, with dissolution at 150 °C resulting in Ce concentrations in solution an order of magnitude higher than for 90 °C.

Dissolution of ThO_2 is complicated by the low solubility of ThO_2 and because the Th^{4+} ion has a tendency to undergo polynucleation and colloid formation. Thus, careful laboratory procedures and a High Resolution ICP-MS is required. In order to optimise analytical work, a set of pre-tests have been conducted during the first year. These tests have shown that dissolution batch tests give measurable Th concentrations, and that solutions with $NaHCO_3$ elevate the Th solubility through carbonate complexation. In

the future, the artificial isotope ^{229}Th could be used to study if the dissolution/ precipitation phenomena occur during the dissolution. The ^{229}Th tracer could also help to avoid the problems with the detection limit of HR-ICP-MS, which is close to the solubility of ThO_2 in basic conditions.

The studies performed on ^{233}U-doped UO_2 samples in natural groundwater are in agreement with previous results, and suggest no effect of the varying intensity of the alpha radiolysis, in spite of the more complex nature of the natural groundwater compared to the previously used synthetic groundwater. Forthcoming work involves a new series of tests using a higher surface area to volume ratio (SA/V =15 m-1).

First principles modelling of CaF_2 surfaces are progressing in collaboration with Stockholm University, using results obtained from confocal profilometry and EBSD as experimental input to the model. The work is focused on establishing surface energies, and an order of surface stability is predicted: (111) > (331)> (110)> (211) > (100); i.e., the (111) surface is the most stable surface. The surface energies of more realistic irregular surfaces are computed by a method involving stepped surfaces. As a result of the investigations, a very general relationship to describe the surface energy of stepped surfaces has been discovered; it is observed that only a few energies of reference planes need to be computed, and all other surface energies can be accurately estimated from a linear relation. Future modelling work involves attempting to describe the dissolution process by studying the binding energies of atoms “sticking out” from the step edge, and by studying chemical reactions on the surface, such as dissociation reaction of a H_2 molecule on the surface of (111) CeO_2. These calculations illustrate that calculating dissociation energies of other molecules such as H_2O should be possible.

REFERENCES

ASTM C 1285-02 (2008), Standard Test Methods for Determining Chemical Durability of Nuclear, Hazardous and Mixed Waste Glasses and Multiphase Glass Ceramics: The Product Consistency Test (PCT). ASTM International.

Atlas Y. and Tel H. (2001) Structural and thermal investigations on cerium oxalate and derived oxalate powders for the preparation of (Th,Ce)O_2 pellets. Journal of Nuclear Materials 298, 316.

Claparede L., Clavier N., Dacheux N., Moisy P., Podor R. and Ravaux J. (2011). Influence of crystallisation state and microstructure on the chemical durability of cerium-neodymium mixed oxides. Inorganic Chemistry 50, 9059-9072.

Fors P., Carbol P., Van Winckel S. & Spahiu K. (2009). Corrosion of high burn-up structured UO_2 fuel in the presence of dissolved H_2. Journal of Nuclear Materials 394.1-8.

Forsyth R. (1987) Fuel rod D07/B15 from Ringhals 2 PWR: Source material for corrosion / leach tests in groundwater. Fuel rod / pellet characterisation program part 1. SKB technical report 87-02.

Forsyth R. (1995) Spent nuclear fuel. A review of properties of possible relevance to corrosion processes. SKB technical report 95-23.

Fourest B., Vincent T., Lagarde G., Hubert S., Baudoin P., (2000). Long-term behaviour of a thorium-based fuel, Journal of Nuclear Materials 282, 180-185.

Gauthier-Lafaye, F., Holliger, P. and Blanc, P-L. (1996). Natural fission reactors in the Franceville basin, Gabon: A review of the conditions and results of a “critical event” in a geologic system. Geochimica et Cosmochimica. Acta, 60, 4831-4852.

Godinho, J.R.A. (2011). Dissolution of fluorite type surfaces as analogues of spent nuclear fuel, Licentiate thesis, Stockholm University.

Godinho J. R. A., Piazolo S., Stennett M. C. and Hyatt N. C. (2011) Sintering of CaF_2 pellets as nuclear fuel analogue for surface stability experiments. Journal of Nuclear Materials 419, 46.

Godinho J. R. A., Piazolo S. and Evins L. Z. (2012). Effect of surface orientation on dissolution rates and topography of CaF_2. Geochimica et Cosmochimica Acta 86, 392-403.

Hubert S., Barthelet K., Fourest B., Lagarde G., Dacheux N., Baglan N. (2001). Influence of the precursor and the calcination temperature on the dissolution of thorium dioxide. Journal of Nuclear Materials 297206-213.

Jiang,Y., Adams J.B. and Van Schilgaarde, M. (2005). Density-functional calculation of CeO_2 surfaces and prediction of effects of oxygen partial pressure and temperature on stabilities. J. Chem. Phys. 123, 064701.

Jones, R.O and Gunnarsson, O. (1989). The density functional formalism, its applications and prospects, Reviews of Modern Physics 61, 689

Lehto J. and Hou X., 2011, Chemistry and Analysis of Radionuclides, Wiley-VCH, Weinheim, Germany.

Metz V., Loida A., Bohnert E., Schild D. & Dardenne K. (2008). Effect of hydrogen and bromide on the corrosion of spent fuel and γ-irradiated UO_2 (s) in NaCl brine. Radiochimica Acta 96, 637-648.

Moon, H.C. (1989). Equilibrium ultrafiltration of hydrolized thorium(VI) solutions, Bulletin of the Korean Chemical.Society 10, 270

Morss L.R., Edelstein N.M. and Fuger J. (ed.), (2010), The Chemistry of the Actinide and Transactinide Elements, 4th edition, Springer.

Neck V., Altmaier M., Müller R., Bauer A., Fanghänel Th. and Kim J. I. (2003). Solubility of crystalline thorium dioxide, Radiochimica Acta 91, 253-262.

Ollila K. (2008a) Solubility of UO_2 in the high pH range in 0.01 to 0.1 M NaCl solution under reducing conditions. Posiva Working report 2008-75, 24 p.

Ollila K. (2008b). Dissolution of unirradiated UO_2 and UO_2 doped with ^{233}U in low- and high-ionic-strength NaCl under anoxic and reducing conditions. Posiva Oy, Olkiluoto, Finland, Posiva Working Report 2008-50, 34 p.

Ollila K. and Oversby V. M. (2005) Dissolution of unirradiated UO_2 and UO_2 doped with ^{233}U under reducing conditions. SKB TR-05-07. Svensk Kärnbränslehantering AB

Ollila K., Albinsson Y., Oversby V. and Cowper M. (2004). Dissolution rates of unirradiated UO_2, UO_2 doped with ^{233}U, and spent fuel under normal atmospheric conditions and under reducing conditions using an isotope dilution method. Posiva Oy, Olkiluoto, Finland, Posiva Report 2004-03, 110 p.

Romano A., Horvarth M. I., and Restani R. (2007) Evolution of porosity in the high-burnup fuel structure. Journal of Nuclear Materials 361, 62.

Shoesmith D. W., (2000). Fuel corrosion processes under waste disposal conditions. Journal of Nuclear Materials 282, 1-31.

SKB (2010). Fuel and canister process report for the safety assessment SR-Site. SKB TR-10-46, Svensk Kärnbränslehantering AB.

Skorodumova, N.V., Ahuja, R., Simak, S.I., Abrikosov, I.A., Johansson, B. and Lundqvist, B.I. (2004). Electronic, bonding, and optical properties of CeO_2 and Ce_2O_3 from first principles. Physical Review. B 64, 115108

Smellie, J and Kalrson F (1996) A reappraisal of some Cigar lake issues of importance to performance assessment, SKB TR 96-08, Svensk Kärnbränslehantering

Vandenborre J., Grambow B. and Abdelouas A. (2010). Discrepancies in Thorium Oxide Solubility Values: Study of Attachment/Detachment processes at the Solid/Solution Interface, Inorganic Chemistry, 29, 8736-8748

Vuorinen U. & Snellman M. 1998. Finnish reference waters for solubility, sorption and diffusion studies. Posiva Oy, Olkiluoto, Finland, Posiva Working Report 98-61, 41 p

Yun Y, and P.M. Oppeneer, P.M. (2011). Ab initio design of next-generation nuclear fuels. MRS Bulletin 36, 178.

Yun Y, Rusz J, Suzuki M-T, and Oppeneer P.M., (2011) First-principles investigation of higher oxides of uranium and neptunium: U3O8 and Np2O5. Phys. Rev. B 83, 075109.